

UTRECHT UNIVERSITY

MASTER THESIS

---

Measuring rainfall using cell phone  
links: classification of wet and dry  
periods using satellites

---

*Author:*

Tessa HAVERKAMP

*Supervisors:*

Aarnout VAN DELDEN (UU)

Aart OVEREEM (KNMI)

Hidde LEIJNSE (KNMI)

July 2013

## *Abstract*

Commercial cellular communication networks can be used for detecting precipitation by looking at the attenuation of the electromagnetic signals transmitted between antennas from microwave links. This attenuation can be translated into a path-averaged rainfall intensity. As the received link signal also fluctuates during dry period, a reference level is needed to represent dry weather in order to calculate the amount of attenuation due to rainfall. This requires a method to separate wet and dry periods.

One classification methodology for wet and dry spells is the "link approach" in which a 15 min interval is labeled wet if the mutual decrease in minimum received powers of nearby links in the same interval exceeds two thresholds. Another methodology is to use ground-based radar rainfall intensities to identify wet and dry spells, called the "radar approach". Conditions can be such that these methods can not be used. Satellites can be a good alternative for wet-dry classification (called the "satellite approach"). Three Meteosat Second Generation products were tested for the Netherlands: Precipitating Clouds, Convective Rainfall Rate and Cloud Physical Properties.

The satellite products were first analyzed separately both visually and quantitatively over a period of four days and compared to gauge-adjusted radar data. The Convective Rainfall Rate product proved to be of limited use for wet-dry classification, so only the Precipitating Clouds and Cloud Physical Properties products were tested as a wet-dry classification for rainfall maps calculated from link data without wet-dry classification or filter for several days. The Precipitating Clouds and Cloud Physical Properties products were combined to use as a wet-dry classification, which improved the results. Finally, link-based country-wide rainfall maps for a 12-day validation set were derived for the Netherlands employing the different wet-dry classification methodologies (link approach, radar approach, satellite approach) with and without use of a filter to remove malfunctioning links. Those maps were compared and validated against gauge-adjusted radar data, considered as ground-truth, showing that the satellite approach could be a good alternative to the link and radar approaches when using a filter.

# Contents

<b>1</b>	<b>Introduction</b>	<b>3</b>
<b>2</b>	<b>Theory</b>	<b>5</b>
2.1	Physics of precipitation . . . . .	5
2.1.1	Cloud formation . . . . .	5
2.1.2	Convective clouds . . . . .	6
2.1.3	Stratiform clouds . . . . .	8
2.1.4	Formation of precipitation . . . . .	9
2.2	Rainfall estimation using microwave links . . . . .	12
2.3	Satellite . . . . .	16
2.3.1	Precipitating Clouds . . . . .	18
2.3.2	Convective Rainfall Rate (CRR) . . . . .	20
2.3.3	Cloud Physical Properties . . . . .	21
2.4	Radar . . . . .	23
<b>3</b>	<b>Methods and data</b>	<b>27</b>
3.1	Comparing Precipitating Clouds, Convective Rainfall Rate and Cloud Physical Properties to radar . . . . .	27
3.1.1	Precipitating Clouds . . . . .	27
3.1.2	Convective Rainfall Rate . . . . .	28
3.1.3	Cloud Physical Properties . . . . .	28
3.1.4	Performance . . . . .	30
3.2	Raw link data . . . . .	32
3.3	Combining Precipitating Clouds and Cloud Physical Properties with raw link data . . . . .	33
3.3.1	Combining Precipitating Clouds with raw link data . . . . .	33
3.3.1.1	No adjustments . . . . .	33
3.3.1.2	With extended rainfall area . . . . .	33
3.3.2	Combining Cloud Physical Properties with raw link data . . . . .	34
3.4	Combining Precipitating Clouds and Cloud Physical Properties as wet-dry classification . . . . .	34
3.5	Adding wet-dry classification using Precipitating Clouds and Cloud Physical Properties to the program . . . . .	34
3.5.1	Data . . . . .	34
3.5.2	Satellite approach . . . . .	36
<b>4</b>	<b>Results</b>	<b>38</b>

---

4.1	Comparing Precipitating Clouds, Convective Rainfall Rate and Cloud Physical Properties to radar . . . . .	38
4.1.1	Precipitating Clouds . . . . .	38
4.1.2	Convective Rainfall Rate . . . . .	40
4.1.3	Cloud Physical Properties . . . . .	42
4.2	Raw link data . . . . .	44
4.2.1	Combining Precipitating Clouds with raw link data . . . . .	44
4.2.2	Combining Cloud Physical Properties with raw link data . . . . .	46
4.3	Combining Precipitating Clouds and Cloud Physical Properties in wet-dry classification . . . . .	47
4.4	Adding the combined wet-dry classification to the program . . . . .	49
4.4.1	Without filter . . . . .	49
4.4.2	With filter . . . . .	51
4.4.3	Comparison to the radar and link approach . . . . .	53
4.4.3.1	No filter . . . . .	53
4.4.3.2	Filter . . . . .	53
<b>5</b>	<b>Discussion</b>	<b>64</b>
<b>6</b>	<b>Conclusions</b>	<b>67</b>
	<b>Bibliography</b>	<b>69</b>

# Chapter 1

## Introduction

Accurate rainfall measurements are very important for example for numerical weather model input, agriculture, water resource management and climatology. Rainfall is primarily measured using weather radars and rain gauges. Unfortunately, weather radar measurements are prone to many sources of errors and the radar requires regular adjustments. Rain gauges can, when well-maintained, provide accurate measurements but these are point measurements with often a low spatial resolution. In case of manual rain gauges, the temporal resolution is also low. In addition, the world coverage of radar and rain gauges is limited to mostly Europe, North America and parts of Asia and Australia. [Messer et al. \[2006\]](#), [Leijnse et al. \[2007\]](#) and [Zinevich et al. \[2009\]](#) were the first to show that commercial microwave cellular communication networks can be an alternative for measuring rainfall. Commercial cellular networks have the benefit that they cover large areas and have a high density, especially in urban areas. The principal idea is that the signal transmitted from one antenna to the other is attenuated by rainfall. This combination of two antennas is called a link. For each 15-minute period the minimum and maximum received power is stored by the cellular communication company for monitoring the network stability. From these powers the attenuation can be calculated which in turn can be translated into a path averaged rainfall depth. [Overeem et al. \[2013\]](#) applied this method of measuring rainfall to the Netherlands, which gave already some promising results.

Also during dry weather fluctuations due to absorption by atmospheric particles are seen in the received link signal. In order to calculate the attenuations caused by rainfall, a reference level representing dry weather has to be defined. Therefore, a method is needed to separate the wet from the dry periods. One way is to use the weather radar (this is called the 'radar approach'). All 15-minute periods where the radar detects no rain are classified as dry. A second method (the 'link approach') uses the received powers of links located near the selected link. When during a 15-minute period the mutual

decrease of the minimum received powers of the surrounding links does not exceed two thresholds this interval is classified as dry [Overeem et al., 2011]. While the link and radar approaches show promising results, these methods can not always be applied due to a lack of weather radar, rain gauges and/or a sufficiently dense commercial cellular network.

In this thesis a novel method is developed to distinguish wet and dry periods for estimating rainfall using commercial microwave links. Geostationary satellites provide almost world wide coverage at an acceptable temporal resolution and could in potential be used to select wet and dry spells on a global scale. The objective of this thesis is the development of a new wet-dry classification scheme using satellite data and to investigate whether it can be used as an alternative for the existing link and radar approaches. This is done for the same location (the Netherlands) and time period as investigated in Overeem et al. [2013].

Chapter 2 discusses the theory behind measuring rainfall using commercial cellular communication networks, weather radars and satellite products. Chapter 3 discusses the methodology for choosing suitable satellite products and how these are applied in the wet dry classification for measuring rainfall employing the commercial cellular communication network. Chapter 4 shows the results of the selected satellite products, the application to the existing routine also used for link and radar approaches and comparison of the performance to previously developed wet-dry classifications. Chapters 5 and 6 discuss the used methodology and draw conclusions from the obtained results.

# Chapter 2

## Theory

This chapter describes the theory behind the research done in this thesis. The formation of clouds and rainfall is discussed in Section 2.1 followed by how rainfall can be measured using a microwave link network in Section 2.2. Section 2.3 discusses the satellite used in the research and the products suitable for measuring rainfall. Section 2.4 finally describes the theory behind measuring rainfall using a weather radar.

### 2.1 Physics of precipitation

The formation of clouds and precipitation are well described in [Summer \[1988\]](#) and [Bierkens et al. \[2008\]](#). These sources are mainly used in the explanations in this section.

#### 2.1.1 Cloud formation

In order to form precipitation clouds have to be present. Cooling moist air to beneath its dew-point temperature  $T_d$  will cause part of the water vapor to condensate, so in order to form clouds, enough moisture has to be available in the air. In addition to enough moisture, cloud condensation nuclei (CCN) have to be present for the moisture to condensate on. Without or with an extremely low density of CNN no condensation can take place. For homogeneous nucleation (condensation in absence of CNN), a supersaturation of over 200% is required [[Bierkens et al., 2008](#)]. Because of this, homogeneous nucleation plays no role in cloud formation. As the presence of CNN is vital for forming clouds it also affects any possible precipitation.

In order for the dew-point temperature to be reached, the moist air has to be cooled. Cooling is mostly caused by an uplift of the air, which can be the result of three processes. First, hot air rises and when air is heated by, for example a warm earth surface,

its density will become lower than the air above it and the warmer air starts to rise. As long as the rising air is warmer than its surroundings it keeps rising (potentially forming convective clouds). Another way is to force the air to rise by for example the presence of a mountain (potentially forming orographic clouds) or when slightly colder and more dense air forces the warmer and less dense air to rise over it (potentially forming stratiform clouds). The last way is when air passes over a relatively rough surface and becomes turbulent [Summer, 1988]. This causes eddies to form in the lowest part of the atmosphere and an exchange between cold and warm air can take place. All three processes are a form of convection, which is defined as the physical motion of molecules in a liquid or gas, in this case in the vertical direction.

As precipitation in the Netherlands originates mostly from convective and stratiform clouds, the formation of only these will be discussed in more detail. More information about orographic cloud formation can be found in Summer [1988].

In order for a cloud to be stable and not evaporate directly after formation, the cloud droplets should have reached a critical size. According to Thomson's formula, a larger supersaturation is required for smaller droplets in order to remain stable as the saturation vapor pressure increases with decreasing radius of curvature. Dissolved material in a water droplet can decrease the saturation vapor pressure with respect to the saturation vapor pressure of a pure water droplet. According to Raoult's law, this reduction is stronger for small droplets than for larger ones. Combining Thomson's formula and Raoult's law yields a critical size beyond which the cloud droplet will remain stable. This critical size is given by Köhler's curve (Figure 2.1) with location of the peak of the curve indicating the critical size.

### 2.1.2 Convective clouds

Assuming the air does not exchange heat with its surroundings, the air rises adiabatically and continues to rise until its temperature is equal to or lower than the temperature of its surroundings. In other words, the air keeps rising while it has a positive buoyancy. Because the rising is adiabatic, the air is also called an air parcel in order to separate it from the environment. This term will be used from now on to indicate the rising air. The buoyancy depends on the internal temperature of the air parcel and the temperature of the surrounding air and is given by

$$B = \frac{(T_a - T_0)g}{T_0} \quad (2.1)$$

with  $B$  the buoyancy in  $\text{m s}^{-2}$ ,  $T_a$  the internal temperature of the air parcel in K,  $T_0$  the external temperature in K and  $g$  the acceleration due to gravity in  $\text{m s}^{-2}$ .

As the pressure decreases with increasing height the pressure on the air parcel also



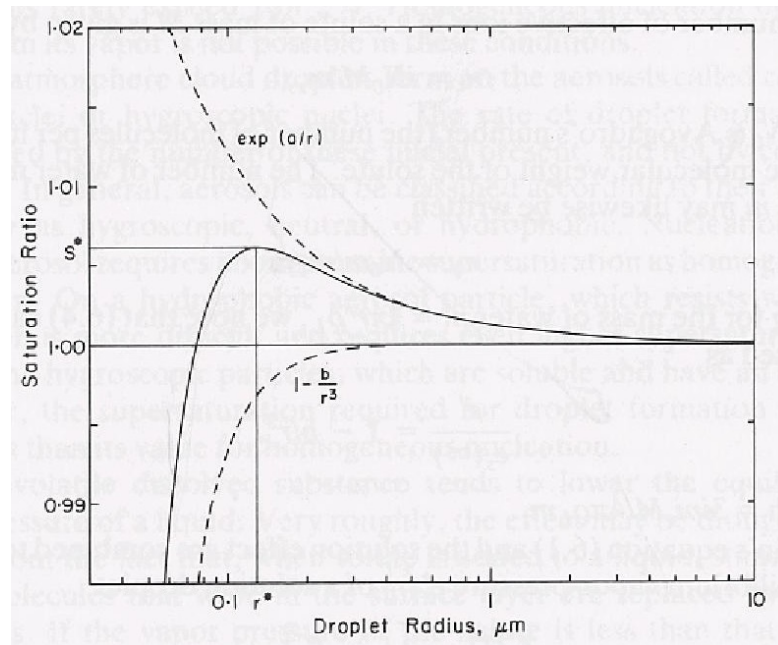


FIGURE 2.1: Köhler's curve showing the droplet radius on the horizontal axis in  $\mu\text{m}$  and the relative humidity on the vertical axis. The location of the peak indicates the critical radius. Source: <http://kkd.ou.edu>

decreases, resulting in an expansion of the air parcel. As energy can not be created or destroyed according to the law of conservation of energy, it can only be converted to another form. As the air parcel rises adiabatically, it is assumed to exchange no heat (which is a form of energy) with its surroundings. Therefore, the energy required for the work done by the expansion of the air, must originate from the air parcel's internal energy. As a result, the internal energy of the air decreases and the air cools. This process is called adiabatic expansion.

As long as the air parcel remains unsaturated the temperature will decrease following the dry adiabatic lapse rate,  $-9.8\text{ }^\circ\text{C km}^{-1}$ . When the air reaches the lifting condensation level, the height at which the air reaches its dew-point temperature and the water vapor in the air starts to condensate, a cloud will begin to form. Above this level, the further decrease in temperature is affected by the release of latent heat by condensation and the saturated adiabatic lapse rate is followed. The temperature of the air parcel at the starting point determines the amount of water vapor it can contain and therefore the amount of condensation and accompanying amount of latent heat. Because of this, the saturated adiabatic lapse rate is not a fixed number but can vary from  $-4.0\text{ }^\circ\text{C km}^{-1}$  for higher temperatures to just above the dry adiabatic lapse rate for low temperatures [Summer, 1988].

The vertical movement of air as a result of the three possible processes mentioned earlier is the dominant way of transporting energy in the atmosphere. As air is a poor conductor, only in the lowest few millimeters the air can be warmed or cooled directly by

the earth surface. Above this small layer convection dominates the transport of energy.

The maximum height a cloud top can reach depends on the vertical temperature distribution of the surroundings. The air parcel keeps rising while positive buoyancy persists. Once the internal temperature of the air parcel equals the temperature of the surroundings, the buoyancy becomes zero and the so called limit of convection is reached, defining the height of the cloud top. Nevertheless, the kinetic energy gained by the rising air can enable the air to rise even above this point, but no water vapor will condensate anymore.

Convective clouds are only formed in an unstable atmosphere where air which is perturbed from its original position will for example continue to rise instead of returning to its original position. In a stable atmosphere, air which is forced upwards will return to its original position instead of continuing to rise.

### 2.1.3 Stratiform clouds

Unlike convective clouds, stratiform clouds can form in a stable atmosphere and are formed by cold air forcing warm air to move over it. This happens at so called fronts, where cold fronts (a cold air mass forcing itself under a slower moving warm air mass) have a steeper so called 'frontal surface' and therefore heavier precipitation than warm fronts (a warm air mass moving over a slower moving cold air mass). A frontal surface rarely has a steepness of more than 2% [Summer, 1988], so warm air is slowly moved upwards and precipitation from stratiform clouds can take place over long periods of time with a low intensity.

Fronts are formed or intensified by frontogenesis, when warm and cold air converge and warm air is forced to rise. The process of frontogenesis is extensively explained in Holton [2004]. In this section frontogenesis is briefly discussed as it is a complex process.

For the generation of frontogenesis, the atmosphere is assumed to be baroclinic (the density changes due to pressure or temperature changes). A statically stable atmosphere is generally in thermal wind balance. This balance is disturbed by frontogenesis, which causes vertical movement of air in the form of ageostrophic circulation to take place in order to readjust to the thermal wind balance. Horizontal shear and/or confluence of geostrophic wind is a frontogenetic effect, disturbing the thermal wind balance.

The so called  $Q$ -vector can give an indication for frontogenesis and is given by

$$\vec{Q} = \left( - \left[ - \frac{\delta v_g}{\delta y} \frac{\delta T}{\delta x} + \frac{\delta v_g}{\delta x} \frac{\delta T}{\delta y} \right], - \left[ \frac{\delta u_g}{\delta y} \frac{\delta T}{\delta x} - \frac{\delta u_g}{\delta x} \frac{\delta T}{\delta y} \right] \right), \quad (2.2)$$

with  $u_g$  and  $v_g$  components of the geostrophic wind in  $\text{m s}^{-1}$  and  $T$  temperature in K. When considering for example a meridional temperature gradient, the first term of the second component shows the effect of horizontal shearing deformation and is the most

important frontogenetic effect. The second term of the second component shows the effect of horizontal stretching deformation. When the magnitude and direction of  $Q$  is shown on a weather map, the effect on the fronts can be identified. When  $Q$  converges, a front intensifies (Figure 2.2) and air ascends. If  $Q$  diverges, a front is weakened and air descends.

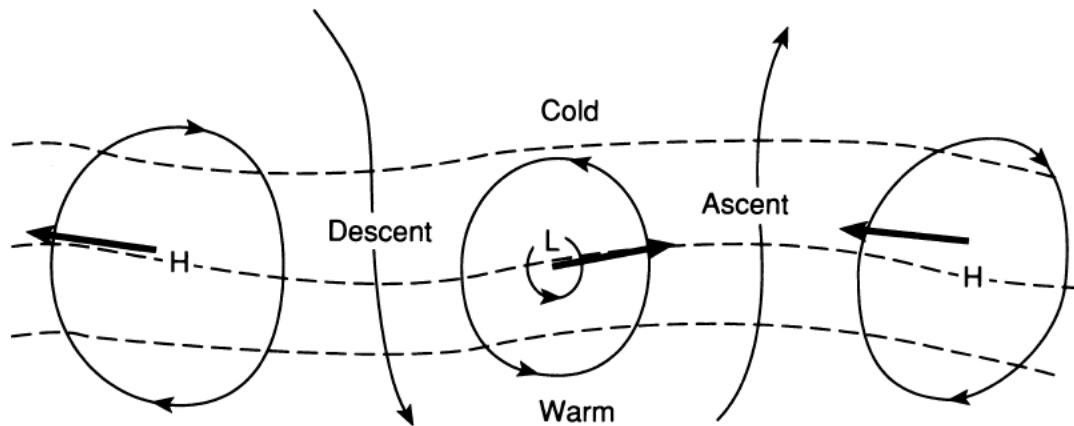


FIGURE 2.2:  $Q$  vectors, indicated by bold arrows, for an idealized pattern of isobars (solid lines) and isotherms (dashed lines) for two anticyclones and a cyclone [Holton, 2004].

#### 2.1.4 Formation of precipitation

As even the large droplets in a cloud are small, they can easily be held aloft by cross-currents and updrafts and evaporate easily in the unsaturated air below the cloud before reaching the ground. Because of this, rain drops should be large enough in order to overcome the updrafts and not evaporate directly below the cloud.

Clouds contains a wide range of droplet sizes ranging from 5 to 30  $\mu\text{m}$  in diameter. The largest and more scarce ones are the most likely to overcome updrafts and absorption and accelerate more quickly to higher terminal velocities than the more numerous smaller ones. These differences in velocities increase the probabilities of collisions between droplets of different sizes. The collisions can be divided into three types, which can influence the type of resulting precipitation: coalescence (collisions of liquid with liquid, producing rain or drizzle), aggregation (solid with solid, producing snow) and accretion (liquid on solid, producing ice grains or hail). When looking at the types of collisions, two types of clouds can be defined. The first one is warm clouds, which have temperatures above 0  $^{\circ}\text{C}$  and only contain water droplets. The second one is cold clouds, having temperatures below 0  $^{\circ}\text{C}$  and consisting of solid ice or supercooled water droplets with temperatures down to -40  $^{\circ}\text{C}$ . Clouds can also consist of separate warm and cold

parts. As warm (parts of) clouds only contain liquid water particles, only coalescence can occur. Accretion is the only collision process in those parts of a cloud where the temperature is below  $-40\text{ }^{\circ}\text{C}$  as no liquid particles are present below this temperature. In the temperature range of  $-40$  to  $0\text{ }^{\circ}\text{C}$  all three collision types can occur as in this range a cloud contains both ice and supercooled water drops.

Although collisions are important for the growth of rain droplets, the Bergeron-

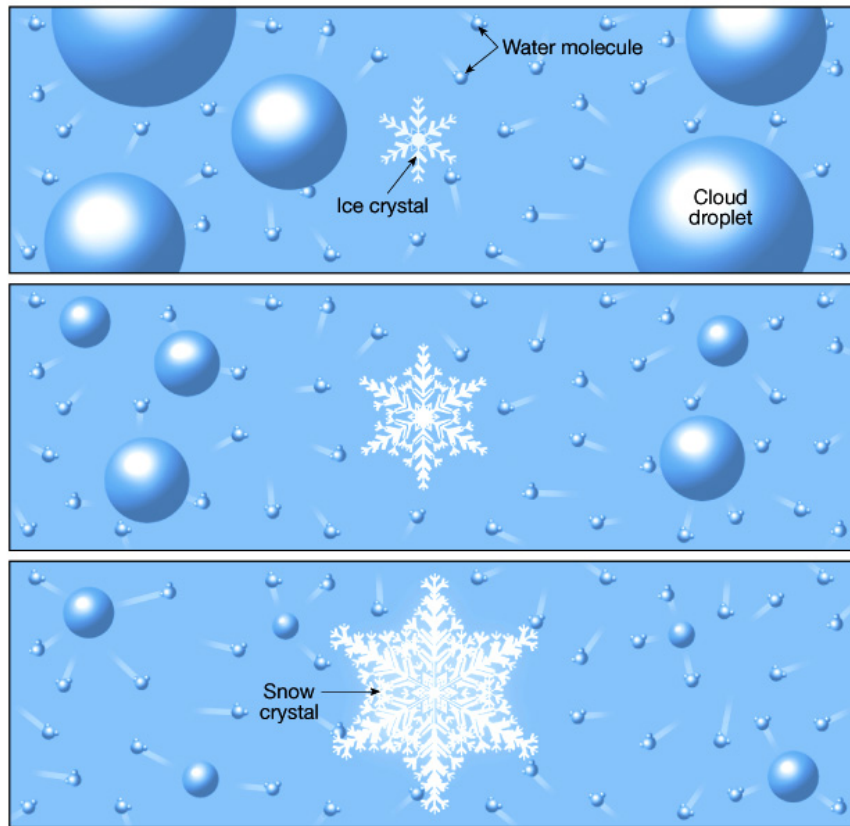


FIGURE 2.3: Schematic representation of the Bergeron-Findeisen process. Due to the air (assumed) to be unsaturated with respect to water, the water droplets will evaporate until the air is again saturated (with respect to water). This will cause the air to be supersaturated with respect to ice, causing the ice particle to grow due to condensation of water vapor. Because of this, the air will be again unsaturated with respect to water and the water droplets will evaporate even further repeating the process until the water droplets are completely evaporated. Source: [www.kennislink.nl](http://www.kennislink.nl)

Findeisen process is seen as an even more important process in the formation of precipitation. To explain the Bergeron-Findeisen process a supercooled water drop and an ice particle are considered as seen in Figure 2.3. As different saturation vapor pressures apply for water and ice, the assumption can be made that the air in the cloud is unsaturated with respect to water and saturated with respect to ice. Because of this, the water drop will evaporate until it is in equilibrium with its environment and the environment will in turn become supersaturated with respect to ice. The water vapor now condenses directly onto the ice particle until the air is again saturated with respect

to ice. The cloud water drop is now out of equilibrium with the surroundings again and evaporates until it is, each time decreasing in mass and in turn increasing the mass of the ice particle. The process continues until the water drop is totally evaporated. Although the process is possible between  $-40$  and  $0$  °C, it is probably most effective in a temperature range of  $-30$  to  $-10$  °C where the highest amount of both ice and water particles are present. Most convectional clouds with a large enough vertical extent will have parts in this effective range. In cases where several stratiform layers exist, like in temperate frontal systems, the upper cold layers will seed ice particles into the lower layers which in turn will use the ice to form large enough raindrops. A water droplet is called a raindrop when it has a diameter larger than  $0.5$  mm [Summer, 1988].

Two processes described above account for most of the precipitation reaching the ground. Nevertheless, not all clouds precipitate as the right temperature, combination and amount of liquid and/or solid particles are required for the formation of precipitation. The vast majority of clouds do not produce any precipitation because of one or more of the following reasons:

1. They are too short lived. Generally, most clouds take 30 to 60 minutes to produce precipitation, where the Bergeron-Findeisen is active for the cases in which precipitation takes the shortest amount of time to be produced.
2. They are too shallow. A reasonable cloud depth is needed in order for vertical motion to take place, increasing the possibilities for cloud droplet growth by collision.
3. They are located too high in the atmosphere. When a cloud is located at a height where the temperatures are low, the amount of available moisture is also low. When precipitation does form from these clouds, the raindrops or ice particles evaporate or sublimate before reaching the ground because of the height. Finally, at these heights the vertical movements is generally low, resulting in tenuous and/or thin clouds.

Precipitating clouds on the other hand have one or more of the following characteristics:

1. They exist for a considerable amount of time, which increases the probabilities of collisions. Because of the long lifetime they are also probably more active including the presence of a considerable vertical motion.
2. They have a significant depth, which increases the opportunities for multiple collisions and the likelihood of containing a considerable thickness with the crucial temperature ranging of  $-40$  to  $0$  °C. Furthermore, a significant depth also favors vertical air motion.

3. When above 0 °C, they have a high liquid water content.

## 2.2 Rainfall estimation using microwave links

The microwave link data used for rainfall measurements originates from the T-mobile commercial microwave link network covering the Netherlands as shown in Figure 2.4 on the right hand side. These links typically have frequencies between 13 and 40 GHz. Each line on this map represent a link as shown on the left hand side of the figure. A link consist of an antenna which emits a microwave signal and a second antenna which receives the emitted signal. When rain is present the signal is attenuated as raindrops scatter some of the energy and another part of the signal is absorbed, leaving less energy to be received than was emitted. The attenuation becomes larger for an increasing number and size of raindrops present along the link. The links are located typically at some tens of meters above the ground and have an average length of 3.1 km. In general, the frequency decreases with increasing link length as longer links need to be affected less by specific attenuation due to rainfall to guarantee continuous up-time.

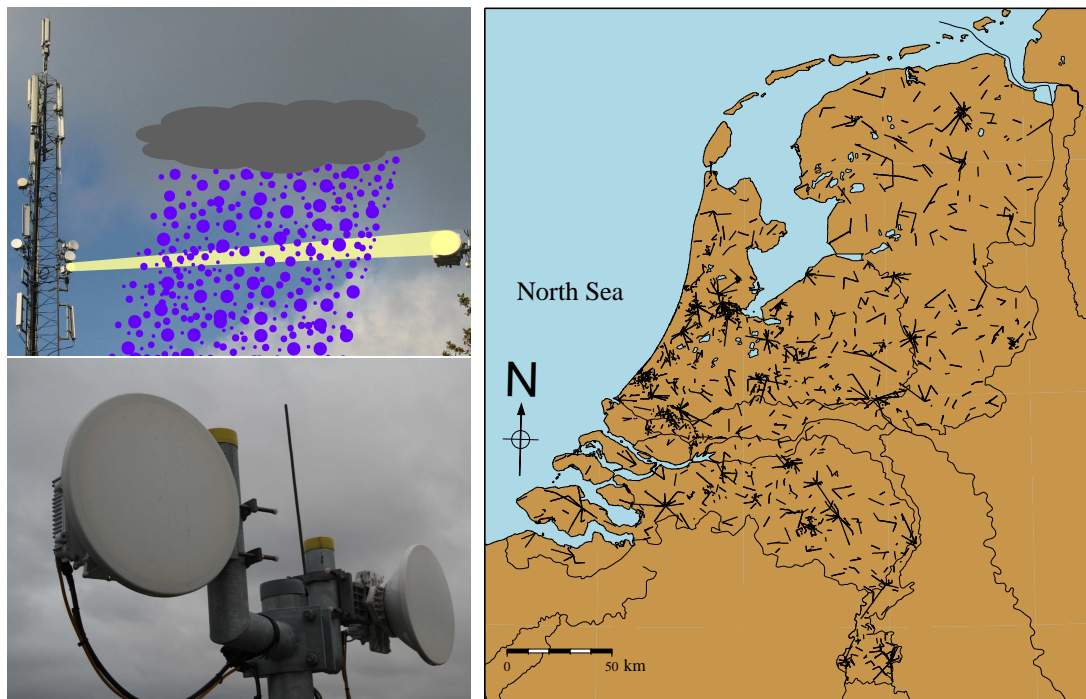


FIGURE 2.4: Microwave links used in the research. (Upper left) attenuation of the microwave signal from a link (Lower left) Antenna from a link (Right) Map of The Netherlands with the locations of the used 1,751 link paths from 2,902 commercial microwave links for the validation (black lines). [Overeem et al., 2013]

By measuring the received power as a function of time, the attenuation due to rainfall can be determined and the path-averaged rainfall over the link can be calculated. The rainfall intensity at one point can be estimated using the following  $R$ - $k$ -relation:

$$R = a k^b, \quad (2.3)$$

with  $R$  the rainfall intensity in  $\text{mm h}^{-1}$ ,  $k$  the specific attenuation of the microwave signal in  $\text{dB km}^{-1}$  and  $a$  and  $b$  are coefficients depending on the frequency, polarization, temperature, water phase, and, if liquid, on the drop size distribution, drop shape and canting angle distribution.

In the case of a microwave link, the decrease in microwave signal power is related to the attenuation by

$$P_{ref}(L) - P(L) = A_m = \int_0^L k(s) ds = \int_0^L \left[ \frac{R(s)}{a} \right]^{\frac{1}{b}} ds, \quad (2.4)$$

with  $P_{ref}$  the reference signal level or baseline in dBm,  $P$  the received signal power in dBm,  $A_m$  the attenuation in dB,  $L$  the length of the link in km and  $s$  the distance along the link in km.

In order to derive rainfall intensities from the received signal powers, it is assumed that the  $R$ - $k$  relation is a good approximation for not only the point-scale rainfall intensity but also the path-averaged rainfall intensity  $\langle R \rangle$  ( $\text{mm h}^{-1}$ ) in the following way:

$$A_m = L \langle k \rangle \approx L \left( \frac{\langle R \rangle}{a} \right)^{\frac{1}{b}}, \quad (2.5)$$

with  $\langle k \rangle$  the path-averaged (specific) attenuation in  $\text{dB km}^{-1}$ .  $\langle R \rangle$  can be expressed as

$$\langle R \rangle = a \left[ \frac{P_{ref}(L) - P(L)}{L} \right]^b. \quad (2.6)$$

The values for  $a$  and  $b$  are derived from measured drop size distributions by [Leijnse et al. \[2009\]](#) and depend mainly on frequency.

A source of error in the calculation of rainfall intensities is the presence of signal fluctuations not related to rainfall. In order to make a correct estimation of the amount of attenuation caused by rainfall a reference level is needed to represent dry weather. In order to calculate this reference level, information is needed about wet and dry periods. Two methods for wet-dry classification are already developed and are called the 'link approach' and the 'radar approach'. When the link approach is used, a 15 minute interval is labeled 'wet' if the mutual decrease in minimum received powers  $P_{min}$  of nearby links within a 15-km radius exceeds two thresholds for that interval as described in [Ovreeem et al. \[2011\]](#). This makes use of the idea that rain has a certain spatial extent. When

rainfall occurs, multiple links are affected and not just one. The radar approach uses unadjusted radar data from the precipitation radars located in De Bilt and Den Helder. If for a 15-minute interval the radar measures a path-averaged rainfall intensity larger than  $0.1 \text{ mm h}^{-1}$ , the current and next time step are declared wet. This is done because the radar measures at about 1.5 km height and with a typical velocity of  $1\text{-}9 \text{ m s}^{-1}$  the raindrops take 3-25 minutes to reach the ground [Overeem].

When the wet and dry periods are determined, the reference signal level  $P_{ref}$  can be determined for each link and 15 minute interval. For each 15 minute interval the minimum and maximum received power  $P_{min}$  and  $P_{max}$  are stored by the network provider in order to monitor the stability of the connection, and taking the average of these two numbers,  $\bar{P}$  is obtained. The reference level is found by taking the median of  $\bar{P}$  for all time steps from the previous 24 hours classified as dry. The reference level is not calculated when less than 10 dry periods of 15 minutes (i.e. 2.5 hours) are available in the previous 24 hours. Using the reference level,  $P_{min}$  and  $P_{max}$  can be corrected

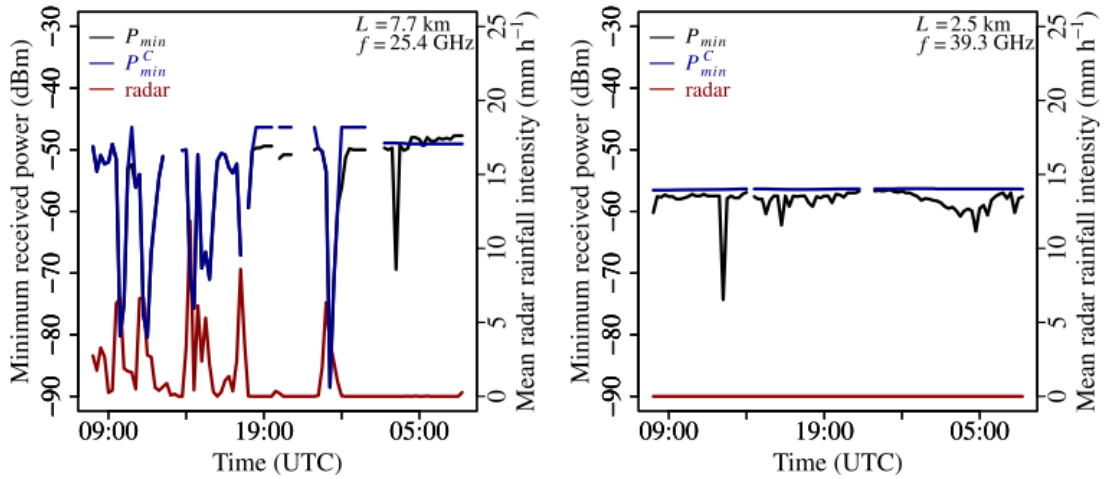


FIGURE 2.5: Minimum received powers (black), corrected minimum received powers (blue), and mean gauge-adjusted radar rainfall intensities (red) for (left) a wet day and (right) a dry day. [Overeem et al., 2011]

using equations 2.7 and 2.8. The corrections remove fluctuations unrelated to rainfall from the signals and the corrected signals  $P_{min}^C$  and  $P_{max}^C$  are used in further analysis. An example of the application of a reference level to calculate  $P_{min}^C$  is shown in Figure 2.5 [Overeem et al., 2011].

$$P_{min}^C = \begin{cases} P_{ref}, & \text{if dry OR } P_{min} \geq P_{ref} \\ P_{min}, & \text{if wet AND } P_{min} < P_{ref} \end{cases} \quad (2.7)$$



$$P_{max}^C = \begin{cases} P_{ref}, & \text{if } P_{max} \geq P_{ref} \text{ OR } P_{min}^C = P_{ref} \\ P_{max}, & \text{if } P_{max} < P_{ref} \text{ AND } P_{min}^C < P_{ref} \end{cases} \quad (2.8)$$

Using the corrected signals, the minimum and maximum attenuation, respectively  $A_{min}$  and  $A_{max}$ , due to precipitation can be calculated:

$$A_{min} = P_{ref} - P_{max}^C \quad (2.9a)$$

$$A_{max} = P_{ref} - P_{min}^C. \quad (2.9b)$$

Using  $A_{min}$  and  $A_{max}$ , the minimum and maximum specific attenuations  $k_{min}$  and  $k_{max}$  can be calculated, followed by the path-averaged rainfall intensity  $\langle R \rangle$ :

$$k_{min} = \frac{A_{min} - A_a}{L} H(A_{min} - A_a) \quad (2.10a)$$

$$k_{max} = \frac{A_{max} - A_a}{L} H(A_{max} - A_a) \quad (2.10b)$$

$$\langle R \rangle = \alpha a k_{max}^b + (1 - \alpha) a k_{min}^b, \quad (2.11)$$

with  $k_{min}$  and  $k_{max}$  the minimum and maximum specific attenuation in  $\text{dB km}^{-1}$ ,  $H$  the Heaviside function (which is zero when  $(A_{min} - A_a) < 0$  for equation 2.10a or  $(A_{max} - A_a) < 0$  for equation 2.10b, otherwise it is one),  $A_a$  the attenuation due to wet antennas in dB and  $\alpha$  a coefficient determining the contribution of  $k_{min}$  and  $k_{max}$  during a 15 minute period.

Before calculating the path-averaged rainfall intensity  $\langle R \rangle$  from  $k_{min}$  and  $k_{max}$ , a filter can be applied to remove local outliers caused by malfunctioning links. This filter excludes a link when the cumulative difference between its minimum specific attenuation  $k_{min}$  and that of surrounding links over the previous 24 hours becomes smaller than  $-130 \text{ dB km}^{-1}$  [Overeem et al., 2013].

Optimal values of  $A_a$  and  $\alpha$  are selected by finding the lowest residual standard deviation with the condition that the mean bias in daily accumulations is smaller than 0.02 mm. The optimization process compares link data from a calibration data set and gauge-adjusted radar data. The residual is the difference between link-based rainfall depths and gauge-adjusted radar rainfall depths. Using the optimal values of  $A_a$  and  $\alpha$ , the mean 15-minute rainfall intensities are calculated for each time step and link of the validation link data set.

The description of the method and the equations shown in this section were largely taken from Overeem et al. [2011].

## 2.3 Satellite

Precipitation can be measured directly by satellites by using a precipitation radar. Unfortunately, not all satellites are suited for this kind of measuring as their orbit is located too high over the earth surface. Therefore information about clouds and precipitation has to be retrieved from the cloud top by using visible and infrared radiation. For example, the brightness temperature and visible reflectance from the top of a cloud can be related to the precipitation below the cloud. The empirical relationship that higher and thicker clouds have a higher probability of occurrence and intensity of precipitation is used in different satellite products. The cloud top height can be found by using the infrared brightness temperature of a cloud and the cloud thickness can be related to the visible reflectance.

As the temporal resolution of the available link data is 15 minutes, the resolution of the used satellite products should ideally be 15 minutes or less. Two types of satellites can be used: geostationary and polar. Geostationary satellites are located over the equator and have the same orbital speed as the rotation speed of the earth. Because of this they are always positioned above the same location on earth and can have a high temporal resolution. Polar satellites pass each pole once every orbit. Because of this difference in orbits, the temporal resolution of polar satellites is much lower than for geostationary satellites. As the temporal resolution of the link data is the same as for geostationary satellites (15 minutes), a geostationary satellite is best suited for the research.

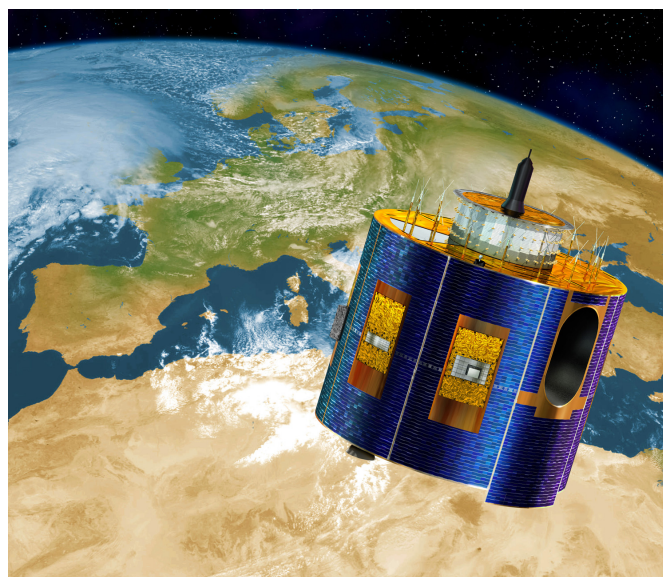


FIGURE 2.6: The Meteosat Second Generation geostationary satellite located over Africa at about  $0^\circ$  latitude and  $0^\circ$  longitude.

The geostationary satellite used in the research is the Meteosat Second Generation or MSG shown in Figure 2.6. This is a European satellite operated by EUMETSAT and is located at a height of about 35800 km over the Gulf of Guinea off the west coast of Africa at about  $0^\circ$  latitude and  $0^\circ$  longitude. The first MSG satellite (METEOSAT-8) was launched in August 2002 and became operational on 19 January 2004. The third MSG satellite (METEOSAT-10) was launched on 5 July 2012 and is now the prime operational meteorological satellite for Europe and Africa. Each Meteosat satellite is expected to remain operational for at least seven years. There are always two operable satellites in orbit, in order to guarantee data continuity in case of a satellite failure. This is necessary as the satellite data is used operationally by meteorologists. A new satellite is launched close to the date at which the elder of the two comes to the end of its on-board fuel.

The MSG satellites cover 20% of the globe including Europe, the North Atlantic and Africa [Roebeling and Holleman, 2009]. Each 15-minute period the complete disc of the earth is scanned by the SEVIRI instrument. The spectral channels used by the SEVIRI instrument are shown in table 2.1 [Schmetz et al., 2002]. The channels have a spatial resolution of  $3 \times 3 \text{ km}^2$  at nadir. For Europe this reduces to about  $4 \times 7 \text{ km}^2$  for a latitude of  $50^\circ \text{ N}$  as the satellite viewing zenith angle is about  $60^\circ$ . These channels are used for providing accurate weather monitoring data.

Channel nr.	Central wavelength ( $\mu\text{m}$ )	Channel observational application
1	0.6	visible light
2	0.8	visible light
3	1.6	near infrared radiation
4	3.9	infrared radiation
5	6.2	water vapor
6	7.3	water vapor
7	8.7	infrared radiation
8	9.7	infrared radiation
9	10.8	infrared radiation
10	12.0	infrared radiation
11	13.4	infrared radiation
12	0.4-1.1	visible light, broadband, high resolution

TABLE 2.1: Spectral channels used by the Meteosat Second Generation SEVIRI instrument.

uses three spectral channels for visible light, one high spatial resolution visual light channel ( $1 \times 1 \text{ km}^2$  at nadir), eight channels for infrared radiation and one channel for near-infrared radiation.

The second instrument on the Meteosat satellites is the GERB (Geostationary Earth Radiation Budget) instrument, which measures the earth radiation budget and is used for better understanding the earth's climate balance. As only SEVIRI data is used in

this research, the GERB-instrument will not be discussed in detail.

The following satellite products are used: Precipitating Clouds (PC), Convective Rainfall Rate (CRR) and Cloud Physical Properties (CPP). Each will be discussed separately in the following subsections. All satellite data used in this thesis has a temporal resolution of 15 minutes. For each time step a snapshot measurement is performed 10 minutes into the 15 minute interval. This means that when a satellite measurement has a time stamp '1400 UTC', the measurement is done at 1410 UTC.

### 2.3.1 Precipitating Clouds

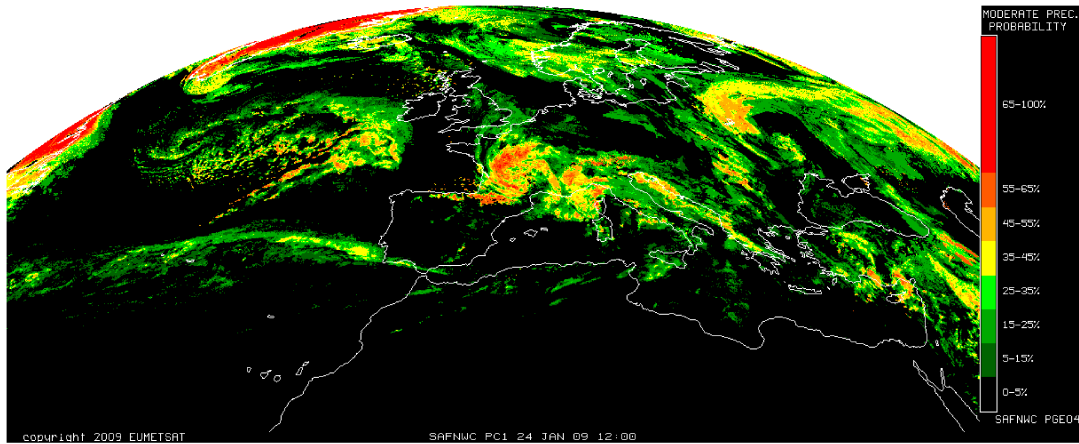
The Precipitating Clouds product gives a precipitation likelihood for intensities larger than  $0.1 \text{ mm h}^{-1}$ . The likelihood ranges from 0 to 100% with intervals of 10%. An example of the output can be seen at the top of Figure 2.7. The rain measured over France by the radar is reflected in the Precipitating Clouds data as an area with a high rainfall likelihood in red, orange and yellow. The (green) areas with a low likelihood are not measured as rain by the radar.

The Precipitating Clouds product consists of two algorithms: one for daytime and one for nighttime. The daytime algorithm uses both the visible light and infrared channels, the nighttime algorithm uses only the infrared channels in the absence of visible light during the night. The condition for using the nighttime algorithm is that the solar zenith angle should be larger than  $80^\circ$ .

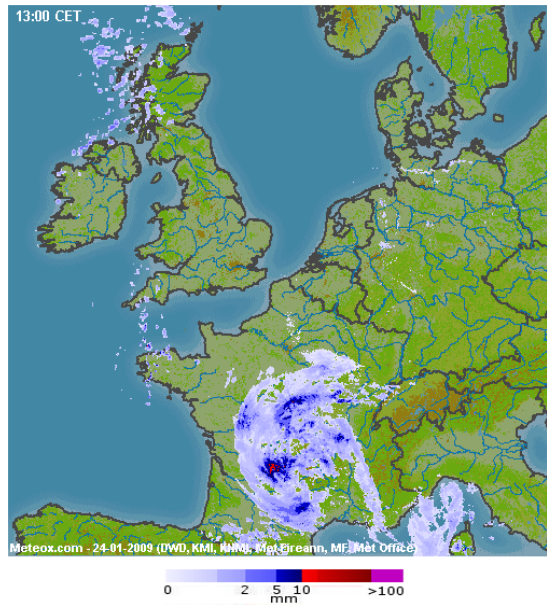
For both day and night, output from another satellite product, the Cloud Type product, is used to determine whether or not a cloud is present in a pixel and if a cloud is detected if it is potentially precipitating. This is done by using a lookup table constructed from French and Hungarian rain gauge data containing precipitation frequencies for different cloud types. When a potentially precipitating cloud is detected, a linear combination of the surface temperature obtained from Numerical Weather Prediction data and those spectral channels with the highest correlation with precipitation are used to construct a Precipitation Index (PI):

$$PI = a_0 + a_1 * T_s + a_2 * T_{10.8} + a_3 * (T_{10.8} - T_{12.0}) + a_4 * |a_5 - R_{0.6}/NIR_{1.6}| + a_6 * VIS_{0.6} + a_7 * NIR_{1.6} + a_8 * T_{6.2} + a_9 * T_{7.3} + a_{10} * T_{3.9}, \quad (2.12)$$

with  $a_0$  to  $a_{10}$  constants which have different values for day and night,  $T_s$  the surface temperature,  $T_i$  the brightness temperatures from the infrared channels with wavelength  $i$ ,  $R_{0.6}$  the reflectivity from the visible light channel with wavelength  $0.6 \mu\text{m}$  and  $R_{1.6}$  the reflectivity from the near infrared channel with a wavelength of  $1.6 \mu\text{m}$ . During the



(A) Precipitating Clouds product



(B) Radar

FIGURE 2.7: (*Top*) Precipitation likelihood given by the Precipitating Clouds product. Green shows precipitation with the smallest likelihood of occurrence, red the precipitation with the highest likelihood of occurrence. Black represents no precipitation. Source: EUMETSAT. (*Bottom*) Precipitation measured by weather radar. Source: [www.buienradar.nl](http://www.buienradar.nl)

night,  $R_{0.6}$ ,  $R_{1.6}$  and  $T_{3.9}$  can not be used as sunlight is required for those channels and the PI reduces to

$$PI = a_0 + a_1 * T_s + a_2 * T_{10.8} + a_3 * (T_{10.8} - T_{12.0}) + a_4 * |a_5| + a_8 * T_{6.2} + a_9 * T_{7.3}, \quad (2.13)$$

where  $a_0$  to  $a_5$ ,  $a_8$  and  $a_9$  have different values than during daytime (equation 2.12).

The precipitation likelihood is determined from the PI and collocated precipitation measurements, like precipitation rates from rain gauges and surface temperatures, using

frequency distributions as is described in detail in [PCt \[2012\]](#).

More detailed information about the Precipitating Clouds product can be found in [PCt \[2012\]](#) and [PCm](#).

### 2.3.2 Convective Rainfall Rate (CRR)

Unlike the Precipitating Clouds product, the Convective Rainfall Rate product gives a precipitation output in terms of the precipitation intensity in  $\text{mm h}^{-1}$ . An example of the output can be seen on the left hand side of Figure 2.8. From comparison to radar data on the right hand side of the figure is seen that much of the radar-detected rain is not shown by the Convective Rainfall Rate product. These missed areas are possibly stratiform rain. Another difference is that the Convective Rainfall Rate product only gives information about convective precipitation and stratiform precipitation associated with convection instead of both stratiform and convective precipitation. This means that only part of all precipitation will be detected by this product. The Convective Rainfall Rate product uses the empirical relationship that higher and thicker clouds have a higher probability and intensity of precipitation. The brightness temperature difference,  $\text{IR}_{10.8} - \text{WV}_{6.2}$  with  $\text{IR}_{10.8}$  the  $10.8 \mu\text{m}$  spectral channel and  $\text{WV}_{6.2}$  the  $6.2 \mu\text{m}$  spectral channel, is used as an indication for deep convective clouds with heavy rainfall. A negative difference has been shown to correspond to convective cloud tops at the tropopause. Also, lightning activity corresponds to convective activity. The Convective Rainfall Rate product has the possibility to employ a lightning algorithm to adjust the Convective Rainfall Rate precipitation pattern. The usage of this algorithm assumes that the higher the spatial and temporal density of lightning occurrence, the stronger the convective activity. This results in a higher probability and intensity of convective precipitation. In order to use the lightning algorithm an information file is required containing information on every lightning occurrence in a time interval.

The used calibration matrices contain a statistical relation between radar rainfall rates and satellite radiation data, where radar data (echo top and rainfall rate from the plan position indicator, PPI, for the Spanish matrices and rainfall rate from pseudo-CAPPI for the Nordic matrices) is compared to satellite data (with the same resolution) for each pixel. From this comparison the rainfall rate is obtained as a function of two or three variables for night and day, respectively, resulting in two calibration matrices: a 2D and a 3D calibration matrix. The satellite channels used in the product are two infrared channels ( $6.2$  and  $10.8 \mu\text{m}$ ) and a visible light channel ( $0.6 \mu\text{m}$ ). The last one is not used during the night because of a lack of visible light. The default threshold for use of the (night) 2D-matrix is a solar zenith angle of  $85^\circ$ . From the calibration matrices,

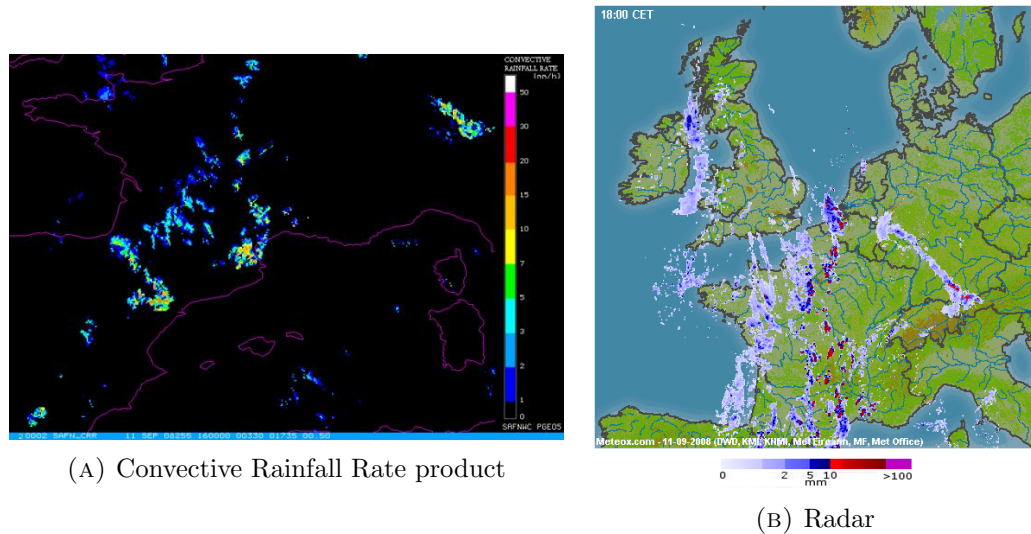


FIGURE 2.8: (*Left*) Precipitation rate in  $\text{mm h}^{-1}$  given by the Convective Rainfall Rate product for Spain and the south of France for 1600 UTC, 11 September 2008. Source: EUMETSAT. (*Right*) Precipitation measured by weather radar. Source: [www.buienradar.nl](http://www.buienradar.nl)

the first estimation for the precipitation intensity is obtained.

For each of the calibration matrices are two versions: a Spanish and a Nordic matrix. For example, the Netherlands are located at a latitude which is not covered by the Spanish or the Nordic matrix. Therefore, in order to obtain the values for the Dutch area, the values from the Spanish matrix are modified by an amount provided by a linear regression between the Spanish and Nordic values depending on the latitude.

Finally, a filter is applied which removes stratiform precipitation not related to convective clouds, by setting the data to zero if all pixels in an area (default is 3 pixels) around the selected pixel have a value lower than a certain threshold (default is  $3 \text{ mm h}^{-1}$ ). This shows that the Convective Rainfall Rate product can detect stratiform precipitation, but this is filtered out as the product is developed for measuring only convective precipitation.

More detailed information about the Convective Rainfall Rate product can be found in [CRR](#).

### 2.3.3 Cloud Physical Properties

The final satellite product used is the Cloud Physical Properties product. This product is developed at KNMI (Royal Netherlands Meteorological Institute) and gives a precipitation rate in  $\text{mm h}^{-1}$ . Unlike the other two products, this product can only be used by day as the algorithm requires data from a visible light channel. A moment is classified as day when the satellite and solar viewing angles are smaller than  $78^\circ$ . An example of the output can be seen on the left hand side of Figure 2.9. The Cloud

Physical Properties product shows resemblances to the radar measurements on the right hand side of the figure. Unlike the Precipitating Clouds and Convective Rainfall Rate products, the Cloud Physical Properties has not yet included a parallax correction in the algorithm. This can be seen in Figure 2.9 from the Cloud Physical Properties rainfall areas to be shifted towards the north compared to the rainfall areas measured by the radar.

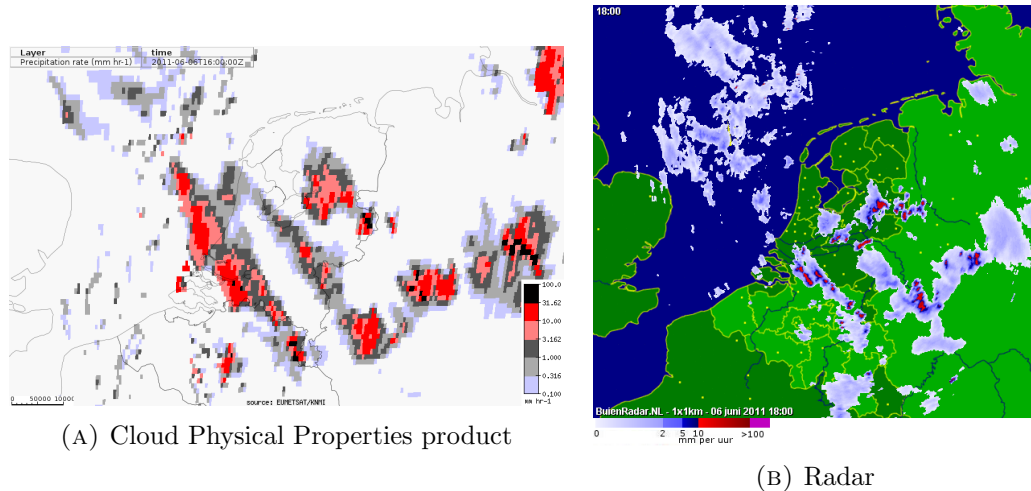


FIGURE 2.9: (*Left*) Map of the precipitation rate for the Netherlands as measured by the Cloud Physical Properties product for 1600 UTC, 6 June 2011. Source: EUMETSAT. (*Right*) Precipitation measured by weather radar. Source: [www.buienradar.nl](http://www.buienradar.nl)

Using a modified cloud detection algorithm developed for MODIS (Moderate Resolution Imaging Spectroradiometer), pixels are declared cloud free, cloud contaminated or cloud filled. For the cloudy pixels the primary cloud properties cloud phase, cloud optical thickness and droplet effective radius are retrieved by iteratively comparing satellite observed reflectances at visible and near infrared wavelengths (respectively 0.6 and 1.6  $\mu\text{m}$ ) to look up tables. These look up tables contain simulated reflectances of water and ice clouds for given optical thicknesses, droplet effective radii and surface albedos. When the reflectances of a pixel correspond to the simulated reflectances of ice clouds and the cloud top temperature is lower than 265 K, the phase 'ice' is assigned to the pixel. All cloudy pixels not meeting both these conditions are assigned the phase 'water'. From the primary cloud properties the cloud water path (CWP) is calculated.

Precipitating clouds are detected using the cloud water path, cloud phase and droplet effective radius. When the cloud water path value in a cloud-containing pixel is larger than  $160 \text{ g m}^{-2}$  a pixel is considered potentially precipitating. Ice clouds meeting this condition are always considered precipitating. Potentially precipitating water clouds ( $\text{CWP} > 160 \text{ g m}^{-2}$ ) with a droplet effective radius larger than threshold  $r_{e,T}$  are considered precipitating, where threshold  $r_{e,T}$  has a value of  $15 \mu\text{m}$ .



For the precipitating clouds, the precipitation rate is calculated using

$$R = \frac{c}{H} \left[ \frac{CWP - CWP_0}{CWP_0} \right]^\alpha, \quad (2.14)$$

with  $R$  the precipitation rate in  $\text{mm h}^{-1}$ ,  $c$  a constant in  $\text{mm h}^{-1} \text{ km}$ ,  $H$  the height of the rain column in  $\text{km}$ ,  $CWP$  the cloud water path in  $\text{g m}^{-2}$ ,  $CWP_0$  the cloud water path offset value in  $\text{g m}^{-2}$  above which  $R$  is calculated and  $\alpha$  a dimensionless constant.

$H$  is calculated from the difference between the warmest cloud top temperature  $CTT_{max}$  over an area of  $100 \times 100$  SEVIRI pixels and the cloud top temperature of the observed pixel ( $CTT_{pixel}$ ). The warmest cloud top temperature over the area is assumed to represent a thin water cloud with a rain column height  $dH$ . This is the minimum height a rain column can have in this area in  $\text{km}$ . The value of  $dH$  is determined by calibrating the algorithm with weather radar observations [Roebeling et al., 2012]. Assuming that the vertical decrease in temperature obeys a wet adiabatic lapse rate of  $6.5 \text{ K km}^{-1}$ ,  $H$  is derived using

$$H = \frac{CTT_{max} - CTT_{pixel}}{6.5} + dH. \quad (2.15)$$

The rain rates are limited to a maximum of  $40 \text{ mm h}^{-1}$  in order to exclude unrealistically high rain rates. No distinction is made between water and ice clouds when calculating the precipitation rate.

More detailed information on the Cloud Physical Properties product can be found in Roebeling et al. [2006], Roebeling and Holleman [2009] and on [http://msgcpp.knmi.nl/mediawiki/index.php/MSGCPP\\_product\\_description](http://msgcpp.knmi.nl/mediawiki/index.php/MSGCPP_product_description).

## 2.4 Radar

KNMI operates two C-band Doppler weather radars, each having a range of  $320 \text{ km}$ : one in De Bilt and one in Den Helder. The radars cover the entire land surface of the Netherlands and scan the atmosphere every 5 minutes with a resolution of  $1 \text{ km}^2$ .

Precipitation is not measured directly but calculated from reflected radiation pulses emitted by the radars. The emitted electromagnetic waves have a frequency of about  $5.6 \text{ GHz}$ , a wavelength close to  $5 \text{ cm}$  and a 3-dB beamwidth of  $1^\circ$ . Reflectivity scans are performed at elevations  $0.3^\circ$ ,  $1.1^\circ$ ,  $2.0^\circ$  and  $3.0^\circ$  over  $360^\circ$  around a vertical axis [Holleman, 2007]. As the use of reflected radiation causes uncertainties to grow larger with increasing distance from the radar, rather good quantitative results of precipitation over the Netherlands can be obtained for a distance up to  $150 \text{ km}$  from the radar. Often gauge adjustment or additional physical corrections are needed. When these are applied,

useful results can be obtained up to ranges of 200 km.

As is described in [Overeem \[2009\]](#), the radar emits an electromagnetic wave of a known power and part of the wave is reflected by precipitation. This reflected power can be used to calculate the radar reflectivity. The distance of the precipitation to the radar can be calculated using

$$r = \frac{ct}{2} \quad (2.16)$$

with  $r$  the distance in km,  $c$  the speed of light in  $\text{km s}^{-1}$  and  $t$  the time delay between emitting and receiving the (reflected) radiation pulse in s.

Assuming the diameter of the scattering precipitation particles is (much) smaller than the wavelength of the radiation emitted by the radar, Rayleigh scattering will be dominant. Using the following relation, the reflected power can be converted to the radar reflectivity factor  $Z$ :

$$Z = C p_r r^2, \quad (2.17)$$

with  $Z$  the radar reflectivity factor in  $\text{mm}^6 \text{ m}^{-3}$ ,  $C$  a radar constant containing information about the emitted power, beam width and wavelength of the radar pulse,  $p_r$  the received power in W and  $r$  the distance to the radar in km.

The reflectivity factor  $Z$  can in turn be transformed to a precipitation intensity  $R$  (in  $\text{mm h}^{-1}$ ) using the relation

$$Z = 200 R^{1.6}. \quad (2.18)$$

The reflectivity is commonly expressed in dBZ instead of  $Z$ , where  $\text{dBZ} = 10 \log(Z)$ . To avoid noise being translated to precipitation, reflectivities lower than 7 dBZ, translating to  $0.1 \text{ mm h}^{-1}$ , are not translated into precipitation. To avoid the influence of hail, the maximum reflectivity is set to 55 dBZ, which translates to  $100 \text{ mm h}^{-1}$  [[Overeem, 2009](#)].

As the radar does not measure the precipitation at the ground, corrections should ideally be applied. This includes for example evaporation of precipitation before it hits the ground and the delay between precipitation being measured by the radar and the precipitation actually hitting the ground due to the height at which the precipitation is measured. The results of the radar are therefore corrected with data from rain gauges. The KNMI has a network of 32 automatic and 326 manual rain gauges. The automatic rain gauges provide information every 10 minutes, the manual rain gauges are handled by volunteers who measure the 24-h precipitation depth every day at 0800 UTC. Daily data therefore runs from 8-8 UTC for all data sets used in this research. Both types of rain gauges are not particularly suited to measure solid precipitation but fortunately this is not a problem as solid precipitation accounts for only a small part of the mean annual precipitation. The spatial resolution for the automatic rain gauges is approximately one measurement per  $1000 \text{ km}^2$ , the manual rain gauges have a resolution of approximately one observation per  $100 \text{ km}^2$  [[Overeem et al., 2009](#)].

Other errors in the measured precipitation are for example the presence of insects, birds, aircrafts or windmills reflecting the emitted radiation, interference or overshooting as mentioned in Hazenberg et al. [2011] and can be seen in Figure 2.10 [Overeem, 2009]. Overshooting causes not all precipitation to be measured by the radar as the precipitation originates from the lower parts of clouds and only a small part of the beam detects the cloud, seeing just the top part of the cloud. The other part of the beam 'shoots over' the cloud, detecting no precipitation. Another cause of error, which is not shown in the figure, is the advection of rainfall. As the precipitation is measured at a mean height of about 1.5 km from the ground, it takes about 5 to 12 minutes for the precipitation to reach the ground. Due to horizontal wind, which is mostly present, and the movement of the clouds themselves precipitation can reach the ground at a different location than where it was measured by the radar. For rain this is typically 1-2 km.

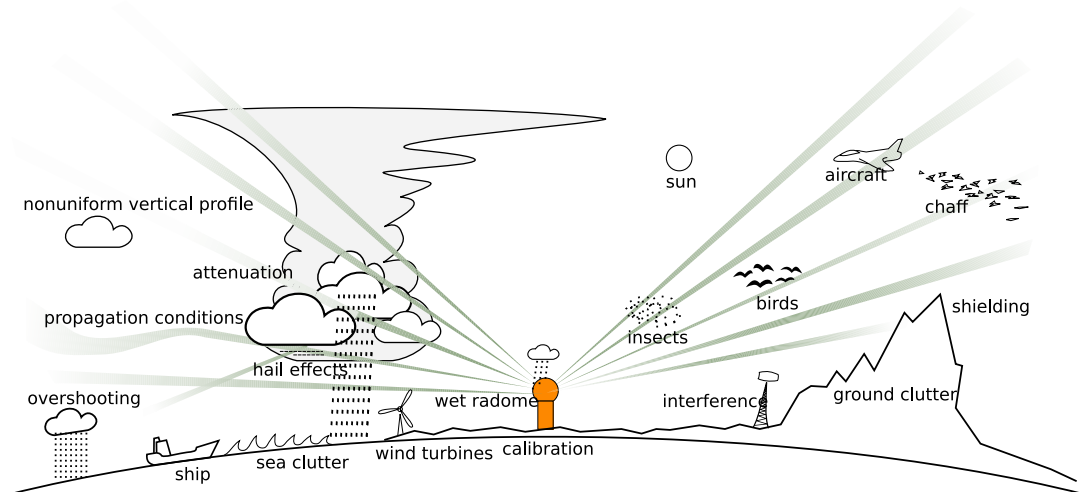


FIGURE 2.10: Source of errors in precipitation measurements by radar. Source: Overeem [2009].

The radar approach in the microwave link measurements described in section 2.2 uses the operational precipitation radar set. The climatological data set used as ground truth in this research is the operational precipitation data adjusted with rain gauge data from that same period. By comparing the collocated radar and gauge observations using equation 2.19 the bias-adjustment factor  $F$  can be determined [Holleman, 2006]. The rainfall intensity measured by the radar is multiplied by this factor  $F$  in order to obtain the gauge-adjusted rainfall intensity.

$$F = \frac{\sum_{n=1}^N R(i_n, j_n)}{\sum_{n=1}^N G_n}, \quad (2.19)$$

with  $R$  the un-corrected radar observations,  $G$  the gauge observations,  $n$  the rain gauge number,  $N$  the number of available rain gauges and  $(i_n, j_n)$  the image coordinates of rain gauge  $n$ .

In order to use the adjusted (climatological) and unadjusted (operational) radar data, for each 15-minute period accumulations of three 5-minute images are made in order to have the same temporal resolution of 15 minutes as the link data.

## Chapter 3

# Methods and data

Three satellite precipitation products are selected which are used for a wet-dry classification in the rainfall measurements using microwave links. Each product is first compared to data from the weather radar for multiple days in 2011. Using this comparison it is decided which products are used in the remainder of this thesis. The suitable products are combined in order to improve results and finally the best combination is plugged into the program also used for the link and radar approaches.

### **3.1 Comparing Precipitating Clouds, Convective Rainfall Rate and Cloud Physical Properties to radar**

#### **3.1.1 Precipitating Clouds**

As said in the previous chapter, the output of the Precipitating Clouds product is a precipitation likelihood and therefore a threshold has to be determined to make a distinction between wet and dry areas. EUMETSAT research proved that a threshold of 20-30% gives the best results, so the thresholds of 10, 20 and 30% are tested for several days in 2011. Below the threshold the area covered by a satellite pixel is labeled dry. All the other cases are labeled wet.

In order to determine which threshold gives the best results a ground truth is needed for which a climatological (gauge-corrected) rainfall radar data set is used. In order to be able to compare the daily link rainfall maps to those of the manual rain gauge network, a day is defined to run from 0800 UTC the previous day to 0800 UTC on the selected day. The comparison between Precipitating Clouds and the radar is therefore done for these periods instead of using midnight as a starting point. When making a first comparison between the satellite products and the radar data, only wet and dry regions

are considered for all products.

As the satellite approach ideally should be applicable all year round, both winter and summer days are investigated including the nights. The investigated days are 20 January and 14, 24 and 29 July 2011 with a 100% data availability.

### 3.1.2 Convective Rainfall Rate

As described in section 2.3.2, the Convective Rainfall Rate product only estimates convective precipitation. It is compared to the radar in the same way as is described for the Precipitating Clouds Product with a threshold of  $0.1 \text{ mm h}^{-1}$  for wet areas. Although the Convective Rainfall Rate gives a precipitation rate as output, just as the Precipitating Clouds product only wet and dry areas are considered in the comparison with radar data. The same days were analyzed as for the Precipitating Clouds Product in order to make the best comparison between the different satellite products. The data availability of the Convective Rainfall Rate product 100%.

### 3.1.3 Cloud Physical Properties

Just like the Convective Rainfall Rate product, the Cloud Physical Properties Product gives a precipitation rate as output, but only wet and dry areas are considered. Before this output can be compared to the radar data a parallax correction has to be applied to the Cloud Physical Properties data. This is included in the Precipitating Clouds and Convective Rainfall Rate products but not yet in this product. Parallax is the apparent shift in the location of precipitation due to the angle under which the satellite looks at the clouds (see Figure 3.1). The figure shows that the parallax depends partly on the cloud height, so the higher the cloud the larger the parallax will be. For the METEOSAT satellite and precipitation in the Netherlands, the precipitation appears to be located more to the north and east with respect to the actual location.

In order to make a parallax correction, the height of the cloud top and the satellite zenith angle must be known. The displacement in the east-west direction turns out to be at most 2.5 km for a 1.25 km high cloud with a satellite viewing angle of  $60^\circ$  [Roebeling and Holleman, 2009] in the most eastern part of the Netherlands where the parallax in this direction is largest. This is clearly smaller than the dimension of a satellite pixel in that direction, so the parallax in this direction is decided to be negligible. Therefore the parallax is assumed to occur only in the north-south direction and using the following relation the displacement to the north can be calculated:

$$\Delta x = h_{cloud} \tan(\theta_s) \quad (3.1)$$

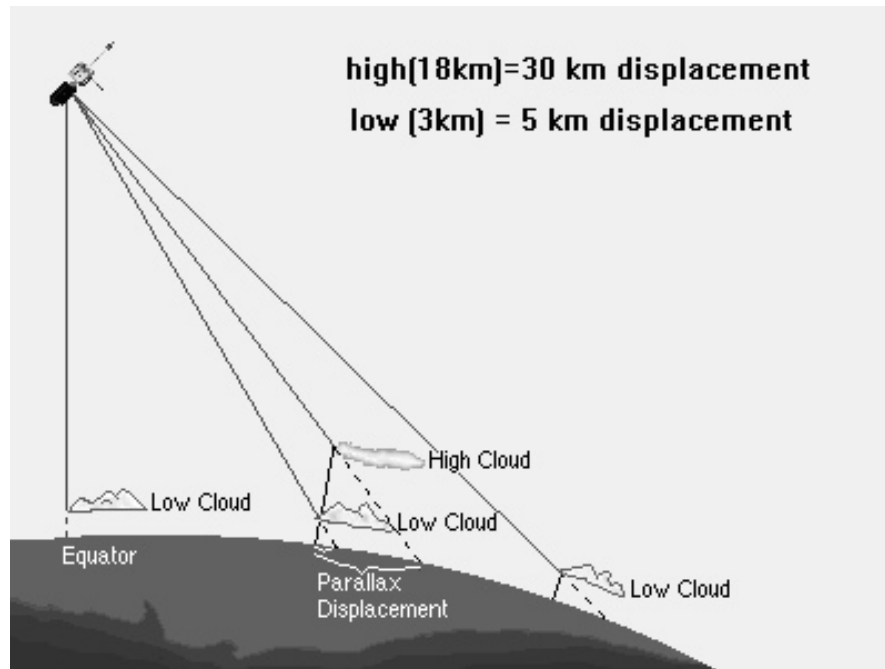


FIGURE 3.1: Error in the location of a cloud due to the fact that the satellite looks at the cloud under an angle. Source: <http://www-das.uwyo.edu/~geerts/cwx/notes/chap02/parallax.html>

In this relation  $\Delta x$  is the displacement due to parallax in m,  $h_{cloud}$  the height of the cloud in m and  $\theta_s$  the satellite zenith angle.

For each pixel in the satellite grid the height of the cloud in that pixel and the satellite zenith angle are known and the parallax correction is made in the following way:

1. First, the amount of precipitation is detected for a pixel. If this is equal to or larger than  $0.1 \text{ mm h}^{-1}$ , the pixel is called precipitating and a parallax correction will be applied to the pixel.
2. Using equation 3.1 the parallax  $\Delta x$  is calculated.
3. The parallax displacement is subtracted from the  $y$ -direction of the coordinates of the pixel, giving the new corrected coordinates of the pixel.
4. The new coordinates are transformed back to a row and column number in the satellite grid and these new row and column numbers determine whether to store the precipitation value in one or two pixels. The corrected data is stored in a new matrix to avoid correction of already corrected data.
5. This procedure is repeated for the whole data matrix with uncorrected data. The corrected data is used for visualization and for the wet-dry classification.

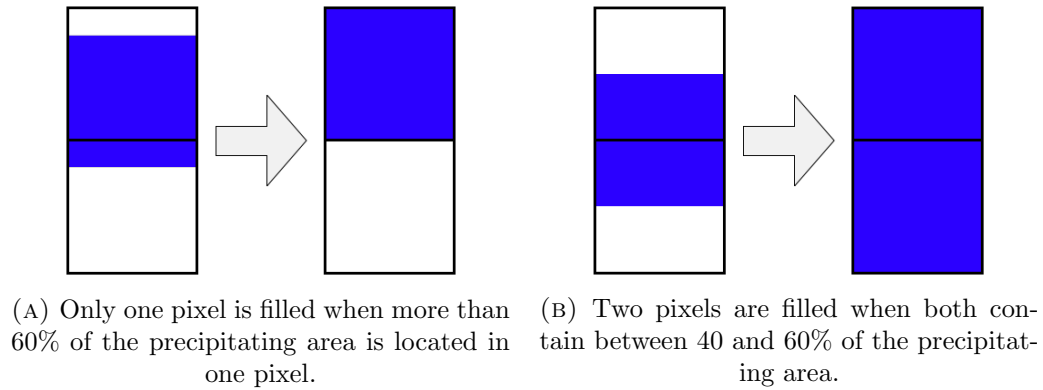


FIGURE 3.2: Projection of a precipitating area to a new parallax corrected location.

The method for deciding if the precipitation is to be placed in one or two pixels in step 4 is shown in Figure 3.2. When more than 60% of the displaced (parallax-corrected) precipitating pixel is located in a pixel, the precipitation is assigned to that pixel only. When the precipitation is spread over two pixels, with each containing 40-60% of the displaced precipitating pixel, both pixels get the value of the original precipitating pixel. It is important to note that precipitation is only assigned to a new pixel when the amount of precipitation already stored in that pixel is lower than the precipitation value that is to be assigned. Because of this, the pixels of the new matrix contain only the largest rainfall value that is assigned to it by the parallax correction. This can possibly slightly decrease the size of the wet areas but no rainfall is removed, it is only displaced.

Looking at Figure 3.1 once more, the presence of (precipitating) clouds can form a shadow over areas where there are no clouds present, and therefore no rainfall and where no data is available as the cloud in front blocks the view of the satellite. As there is no certainty of whether precipitation is present at those locations, the assumption is made that those areas are wet in order to increase the Probability Of Detection. Therefore, not only the new corrected position is considered wet, also the original position and all intermediate pixels are considered wet, getting the original rainfall value assigned to them (see Figure 3.3). In this way, the probability to detect rainfall is likely to increase as more pixels are considered wet.

### 3.1.4 Performance

In order to not only qualify but also quantify how well satellite products and radar compare, statistics are needed. These are calculated by comparing the pixels of the radar grid to the pixels in the satellite grid. As the radar and satellite products use



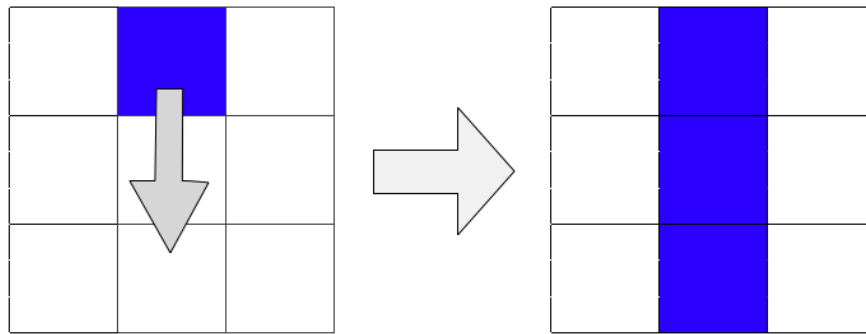


FIGURE 3.3: When a precipitating pixel is displaced using the parallax correction, shown on the left side, the new position and all pixels between the old and new position get the value of the old precipitating pixel.

different grids,  $1 \text{ km} \times 1 \text{ km}$  in case of the radar and about  $4 \text{ km} \times 7 \text{ km}$  over Europe for the satellite, all data has to be represented in the same grid in order to make a good comparison. As it is more convenient to translate a high resolution grid to a lower resolution grid, the radar data is transformed to the satellite grid. How this is done is shown schematically in Figure 3.4.

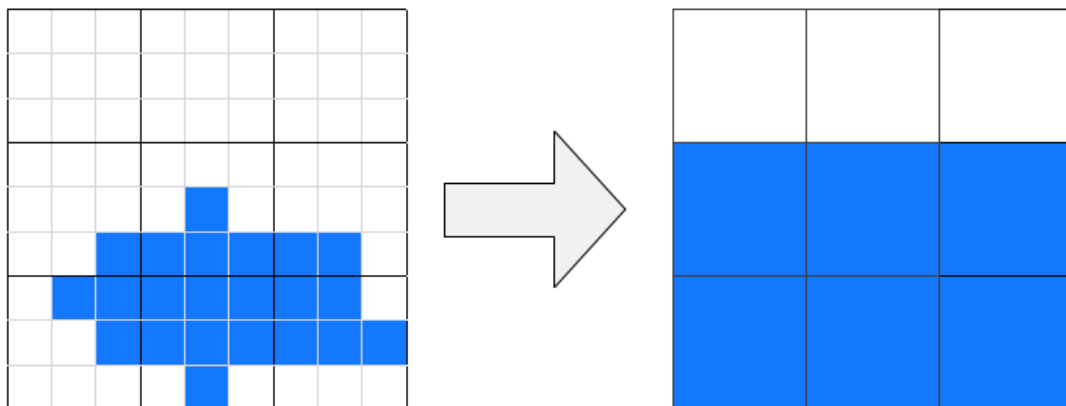


FIGURE 3.4: Schematic view of the transformation of radar data from the radar grid to the satellite grid. The large squares indicate the pixels of the satellite grid. The small squares represent the smaller pixels of the radar grid. Precipitation is indicated in blue.

For each satellite pixel it is determined which radar pixel centers are located in that same area. When at least one of those radar pixels are indicated as wet, the whole pixel in the satellite grid is set to wet. When none of the radar pixels are wet, the pixel is labeled dry. The left hand side of Figure 3.4 shows the radar data before transformation with an overlay of the satellite resolution. On the right hand side the radar data is translated to the satellite grid.

After transforming the radar data to the satellite resolution the following terms can be used in the comparison of the satellite data to the gauge-adjusted radar data: For

	Radar dry	Radar wet
Satellite dry	correct negative	miss
Satellite wet	false positive	hit

TABLE 3.1: Comparing satellite data to radar data

example, when a pixel is wet according to both the satellite data and the radar data, this is called a hit. When both are labeled dry, this is a correct negative. Using the terms from Table 3.1, the False Alarm Ratio (FAR), Probability Of Detection (POD) and accuracy can be calculated.

$$\text{FAR} = \frac{\text{false positive}}{\text{false positive} + \text{hits}} \quad (3.2)$$

$$\text{POD} = \frac{\text{hits}}{\text{hits} + \text{misses}} \quad (3.3)$$

$$\text{Accuracy} = \frac{\text{hits} + \text{correct negatives}}{\text{total}} \quad (3.4)$$

The FAR shows how much of the area indicated wet by the satellite is actually dry according to the radar. The POD shows the likelihood of precipitation measured by the radar to be measured by the satellite as well. The accuracy shows how much of the area measured by the radar is correctly identified by the satellite. These statistics are made for all three satellite products in order to see quantitatively the performance of each product over the different days. In the ideal situation the FAR is 0, having no false alarms, and the POD and accuracy both 1, all wet areas detected by the satellite and all areas declared correctly dry/wet. In the case of the Cloud Physical Properties product, data is only available during daytime so only daytime statistics can be calculated.

## 3.2 Raw link data

When investigating the improvement in rainfall measurements by using the different satellite products as a wet-dry classification, raw link data is used to directly calculate rainfall without applying any wet-dry classification or filter to the calculations. The statistics of the results are calculated in the same way as was done for the different satellite products in Section 3.1. The only difference with the satellite products is that the results from the link data are represented in the radar grid. Therefore no translation to another grid has to be made for the link data and the rainfall maps calculated from the raw link data can be compared directly to the radar rainfall maps.

### 3.3 Combining Precipitating Clouds and Cloud Physical Properties with raw link data

Using the method for selecting useful satellite products described in Section 3.1 it is concluded that the Convective Rainfall Rate product is not suitable for the purpose of a wet-dry classification as the Probability Of Detection proved to be too low for all investigated days. This is described in more detail in Section 4.1.2. Therefore only the Precipitating Clouds and Cloud Physical Properties products are tested for wet-dry classification on the raw link data.

#### 3.3.1 Combining Precipitating Clouds with raw link data

Light precipitation at the edge of the cloud is difficult to detect (Roebeling [2008] and Amorati et al. [2000]) and is therefore easily missed. The results of a satellite-based wet-dry classification can possibly improve when the rainfall area detected by the satellite is extended by one satellite pixel. The situations without and with using extended rainfall areas are therefore investigated.

##### 3.3.1.1 No adjustments

First, the Precipitating Clouds data is used directly as wet-dry classification without making any adjustments to the satellite data. A threshold of 20% is used for rainfall, which turned out to give the best results using the method from Section 3.1.1. For each link pixel it is determined in which satellite pixel it is located and whether that pixel is wet or dry. When both the link and corresponding satellite pixel are wet, the rainfall value of the link pixel is maintained. A link pixel is considered wet if the rainfall depth is equal to or larger than 0.1 mm. When only one of the two or none is wet, the link pixel is set to dry.

The results of this first application of a wet-dry classification are tested against the radar data in the same way as is described in Section 3.2. As the link data has the same grid as the radar data, the comparison can be made relatively easy.

##### 3.3.1.2 With extended rainfall area

Satellites usually do not measure the outer area of a precipitating cloud well as this is not as high and active as the inner region, whereas precipitation is still present there. Therefore the precipitating area as measured by the Precipitating Clouds product is

extended. When a pixel is declared wet according to the Precipitating Clouds data, all eight surrounding pixels are classified as wet as well. The results are then again compared to the radar data in the usual way.

### **3.3.2 Combining Cloud Physical Properties with raw link data**

The Cloud Physical Properties data including the parallax correction is used as wet-dry classification on the raw link data in the same way as was done for the Precipitating Clouds data. The situation with an extended precipitating area is also investigated in the same way in order to see if this will improve the results.

## **3.4 Combining Precipitating Clouds and Cloud Physical Properties as wet-dry classification**

As the purpose of the wet-dry classification is to detect as much of the radar detected rainfall as possible, the Precipitating Clouds and Cloud Physical Properties products are combined to use as a wet-dry classification in order to increase the probability of detecting rainfall. The combination of the products is applied directly to the raw link data. A (link) pixel is declared wet if the link data and at least one of the satellite products exceed their threshold for rainfall. This was 0.1 mm for both the link data and the Cloud Physical Properties product and 20% for the Precipitating Clouds product. For both satellite products the precipitating areas have been extended.

## **3.5 Adding wet-dry classification using Precipitating Clouds and Cloud Physical Properties to the program**

### **3.5.1 Data**

The link and gauge data used in this thesis are the same as described in [Overeem et al. \[2013\]](#). The received minimum and maximum received signal level data were obtained from a commercial microwave link network covering the Netherlands (having a surface area of 35.500 km<sup>2</sup>). Figure 3.5 shows the locations of the links used in this thesis.



FIGURE 3.5: Locations of the about 2400 links used in this research.

The about 2400 links have frequencies of about 13-40 GHz and an average length of 3.1 km. The minimum and maximum received powers are available over 15-minute intervals and have an accuracy of 1 dB, based on 10-Hz sampling. The links have a single frequency and transmit vertically polarized signals.

A 12-day calibration and a 12-day validation data set are used. Table 3.2 shows the days from June to September 2011 which are included in the data sets. Removing malfunctioning links by applying the -130 dB filter for the satellite approach gives a reduction of 1.28% in the number of links used in the validation data set compared to the number of links used for the satellite approach without filter.

The rain gauge data used for the gauge-adjusted radar data is obtained from about 325 daily manual and about 32 10-minute automatic rain gauges from KNMI. The data of the manual rain gauges are collected daily at 0800 UTC.

The satellite data are obtained at a 15-minute temporal resolution. The data availability for the calibration set is 99.48% and 99.96% for respectively the Precipitating Clouds and Cloud Physical Properties products. For the validation set the data availability is 99.13% and 99.09% for respectively the Precipitating Clouds and Cloud Physical Properties products.

Calibration	Validation
7 June 2011	11 June 2011
16 June 2011	7 August 2011
17 June 2011	8 August 2011
29 June 2011	9 August 2011
13 July 2011	14 August 2011
14 July 2011	19 August 2011
15 July 2011	23 August 2011
17 July 2011	26 August 2011
18 July 2011	28 August 2011
24 July 2011	7 September 2011
25 July 2011	8 September 2011
29 July 2011	11 September 2011

TABLE 3.2: Days in the (*Left column*) calibration and (*Right column*) validation data sets.

### 3.5.2 Satellite approach

The combination of satellite products as described in the previous section is now implemented in the routine of calculating rainfall from link data described in Section 2.2. For each link is determined which 15-minute intervals are dry by using the Precipitating Clouds and Cloud Physical Properties products before calculating the reference level. An interval is classified 'dry' when both products detect no rain: a likelihood  $\geq 20\%$  for the Precipitating Clouds product and a rainfall intensity  $\geq 0.1 \text{ mm h}^{-1}$  for the Cloud Physical Properties.

Using a calibration data set of 12 days (June, July 2011), the optimal values for  $A_a$  and  $\alpha$  are obtained as described in section 2.2 and the optimized routine is then used to calculate rainfall depths for the 12-day validation set (June, August and September 2011). After the rainfall depths are calculated for the different links, the data is interpolated using ordinary kriging in order to obtain rainfall maps for the total area covering the Netherlands [Overeem et al., 2013].

Daily rainfall maps are obtained for each day of the validation set by accumulating all the 15-minute rainfall maps for each day. Furthermore, scatter plots are constructed for the 15-minute and daily rainfall maps with spatial resolutions of  $81 \text{ km}^2$  and  $1 \text{ km}^2$  respectively in order to quantify the performance of the satellite approach. When the scatter plots are constructed, the mean radar and link rainfall depths, the coefficient of variation  $CV$  and the coefficient of determination  $\rho^2$  (in this case the squared Pearson correlation coefficient) are calculated. The coefficient of variation  $CV$  is the ratio of the standard deviation of the residuals and the mean, so the lower the  $CV$ , the lower the relative spread in the rainfall depth. The coefficient of determination  $\rho^2$  can have any value between 0 and 1 and the higher the value of  $\rho^2$ , the higher the correlation between

---

two variables, in this case link and gauge-corrected radar data. The mean radar and link rainfall depths are calculated by using only the rainfall values equal to or larger than 0.1 mm.

Both the situations without and with the -130 dB filter are studied for the satellite approach. Finally, the results from the satellite approach are compared to the link and radar approaches.

# Chapter 4

## Results

This chapter shows first the results of the selection of useful satellite products. The suitable products are then applied as wet-dry classification on link data which has already been translated to rainfall maps without a wet-dry classification or filter applied and the resulting rainfall maps are compared to the gauge-adjusted radar rainfall maps. The applicable satellite products are then combined in one wet-dry classification and subsequently used on the just described raw link data. Finally, the combined wet-dry classification is employed in the program also used for the link and radar approaches, forming the satellite approach. After calibration, rainfall maps are calculated using the satellite approach for the validation data set with and without filter. These maps are compared to the existing wet-dry classifications.

### 4.1 Comparing Precipitating Clouds, Convective Rainfall Rate and Cloud Physical Properties to radar

#### 4.1.1 Precipitating Clouds

For multiple days (19 January and 13, 23 and 28 July 2011) the satellite data is visualized and compared to a gauge-adjusted radar data set, often called radar hereafter. As not all the visualized data can be shown in this report, Figure 4.1 shows one moment at which the differences in areas declared wet by the different thresholds are clearly visible. The radar image shows no precipitation over sea as it has a sea mask applied to it allowing only precipitation to show over the land surface of the Netherlands. Note that the time shown in the satellite pictures indicate the start of the 15 minute measuring period, but the actual measurement is done 10 minutes into that 15 minute period. In this case, the measurement by the satellite is done at 1455 UTC. Looking at the 10% threshold first,



large precipitating areas are detected by the satellite product including large areas where the radar detects no precipitation. This may result in too much link data incorrectly classified wet and therefore few links to be used to calculate the reference level when using this threshold in a wet-dry classification. When using the 20% threshold, the precipitating areas seen by the satellite are also large, but not as large as for the 10% threshold. For the 30% threshold a clear decrease in the size of the precipitating areas is observed. Much less precipitation that is detected by the radar is also detected by the satellite. This may result in too much link data associated with rainfall being rejected in case of application in a wet-dry classification.

Table 4.1 shows the mean performance for the different thresholds 10, 20 and

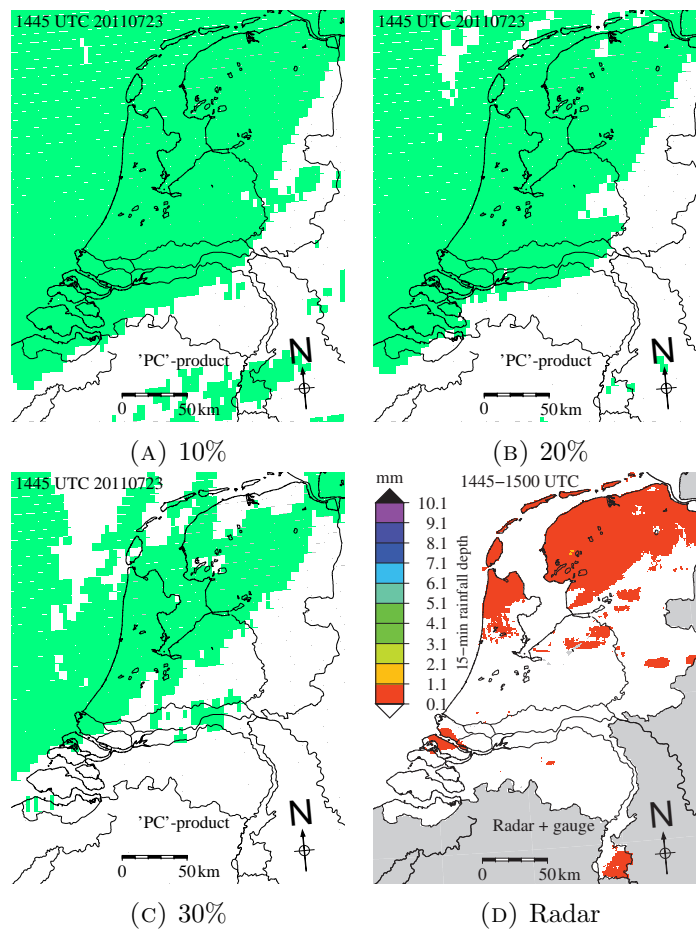


FIGURE 4.1: Wet and dry regions as detected by the Precipitating Clouds product using the (A) 10%, (B) 20% and (C) 30% thresholds for precipitation compared to the (D) gauge-adjusted radar rainfall map for 1445 UTC on 23 July 2011. Precipitation is shown in green for the Precipitating Clouds product. The radar shows the 15-minute rainfall depth in mm.

30% calculated over the land surface of the Netherlands in terms of False Alarm Ratio, Probability Of Detection and accuracy averaged over the investigated days. The days are not shown separately for the different threshold in order to view the overall performance

of the thresholds.

Threshold	False Alarm Ratio	Probability Of Detection	Accuracy
10%	0.39	0.57	0.80
20%	0.32	0.47	0.82
30%	0.28	0.21	0.78

TABLE 4.1: Precipitating Clouds performance over 20 January, 14, 24 and 29 July 2011 in terms of False Alarm Ratio, Probability Of Detection and accuracy.

The 10% threshold has the largest Probability Of Detection, but also the largest False Alarm Ratio. This makes sense as this threshold shows the largest precipitating area, which has advantages (much precipitation is detected correctly) but also disadvantages (more false alarms). When setting the threshold to 20%, both the Probability Of Detection and the False Alarm Ratio decrease and the accuracy increases. Increasing the threshold to 30% results in a large decrease in Probability Of Detection and smaller decreases in the False Alarm Ratio and accuracy. Looking just at the False Alarm Ratio and the Probability Of Detection no clear decision can be made on which threshold is most useful. The ideal case of a high Probability Of Detection and a low False Alarm Ratio is not seen for any of the thresholds but based on the accuracy and the visualized results, the 20% threshold is considered the best and used in the rest of the research. Although the Probability Of Detection is not high for this product, the accuracy is at least 78% and the False Alarm Ratio at most 39% allowing the product to be possibly useful for wet-dry classification. Table 4.2 shows the performance of the 20% threshold for the four investigated days, whose values for the False Alarm Ratio, Probability Of Detection and accuracy depend largely on the investigated day. Promising is that the accuracy is always at least 69%.

Day	False Alarm Ratio	Probability Of Detection	Accuracy
20 January	0.15	0.30	0.91
14 July	0.59	0.58	0.69
24 July	0.16	0.73	0.73
29 July	0.36	0.27	0.94

TABLE 4.2: Performance of the 20% threshold for the Precipitating Clouds product over 19 January, 13, 23 and 28 July 2011

#### 4.1.2 Convective Rainfall Rate

The Convective Rainfall Rate product is evaluated for the same days as were used in the previous section. The performance is clearly worse than that of the Precipitating Clouds product. During winter, none of the rainfall measured by the radar was detected by the

Convective Rainfall Rate product (Figure 4.2). The Convective Rainfall Rate product only measures convective precipitation, as is the objective of the product, whereas winter precipitation is mainly stratiform. Hence, the Convective Rainfall Rate Rate product seems to be unsuitable as wet-dry classification during winter.

Despite the precipitation being more of a convective nature during summer, still

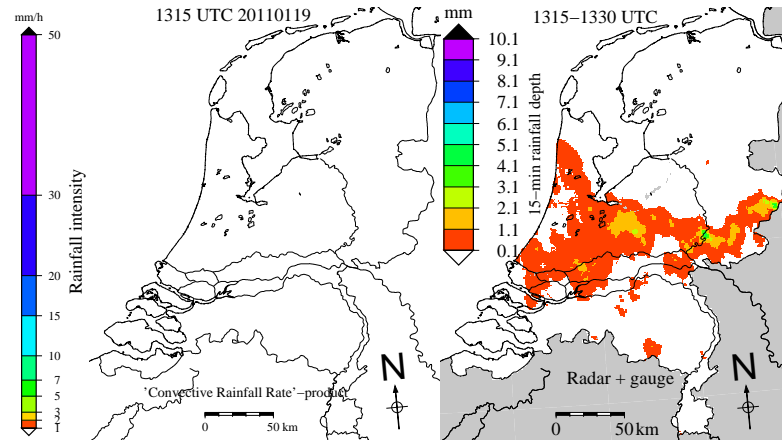


FIGURE 4.2: Rainfall intensity measured by the Convective Rainfall Rate product in  $\text{mm h}^{-1}$  (left) and the 15-minute rainfall depth measured by the gauge-adjusted radar in mm (right) for 1315 UTC on 19 January 2011.

not all precipitation is detected correctly during this season as can be seen in Figure 4.3. Precipitation is now detected, but almost none of the precipitation measured by radar is correctly located by the satellite product.

Table 4.3 shows the performance of the Convective Rainfall Rate product. The

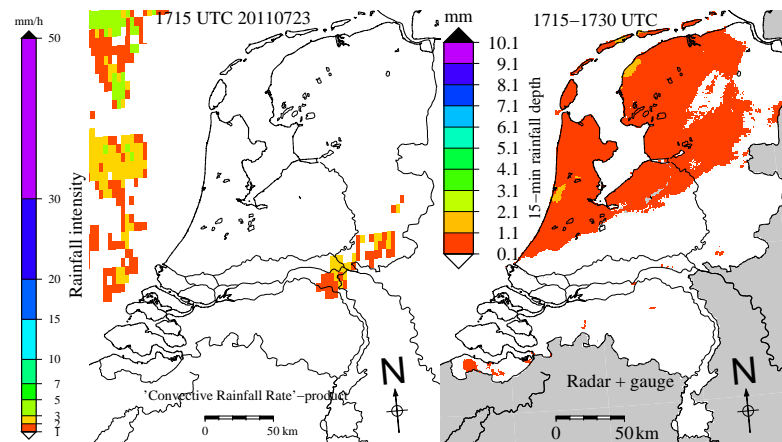


FIGURE 4.3: (Rainfall intensity measured by the Convective Rainfall Rate product in  $\text{mm h}^{-1}$  (left) and the 15-minute rainfall depth measured by the gauge-adjusted radar in mm (right) for 1715 UTC on 23 July 2011.

Probability Of Detection is almost negligible, never exceeding 5%. The accuracy on 19 January is high and the False Alarm Ratio and Probability Of Detection are both zero. This indicated that the accuracy alone is not a good measure of the performance as it in this case only reflects the correctly detected dry periods, which are more numerous

than wet periods. Not much precipitation was detected by the radar on this day and as the Convective Rainfall Rate product could not detect any precipitation all dry areas are correctly classified as dry. On 13 July, the areas that are classified as wet by the satellite product are often located at dry areas, according to the radar, resulting in a high False Alarm Ratio.

From the Figures and statistics for this satellite product, it can be concluded that

Day	False Alarm Ratio	Probability Of Detection	Accuracy
20 January	0.00	0.00	0.93
14 July	0.65	0.01	0.81
24 July	0.38	0.05	0.52
29 July	0.30	0.04	0.96

TABLE 4.3: Convective Rainfall Rate performance over 19 January, 13, 23 and 28 July 2011 in terms of False Alarm Ratio, Probability Of Detection and accuracy.

this product is not suited for wet-dry classification. Therefore this product is discarded.

### 4.1.3 Cloud Physical Properties

Unlike the first two satellite products the Cloud Physical Properties product is only available during daytime. All statistics below therefore only reflect the daytime situations, but this still gives a good indication of the usability of the product. In Section 4.2 the daytime statistics are shown for the different satellite products combined with raw link data in order to give a better comparison between the products.

As the Clouds Physical Product algorithm has not yet included a parallax correction, this has been implemented as described in Section 3.1.3. The effect of implementing the parallax correction can be seen in Figure 4.4.

By declaring all pixels in the parallax shift of a wet pixel also as wet, the total amount of pixels in the grid that is declared wet significantly increases. The probability of detecting precipitation could therefore increase, which is good when using the Cloud Physical Properties product as a wet-dry classification, but the amount of wrongly defined wet pixels can also increase. The ability of the Cloud Physical Properties product including the necessary parallax correction to detect wet and dry periods can be seen in Table 4.4 for the available satellite data:

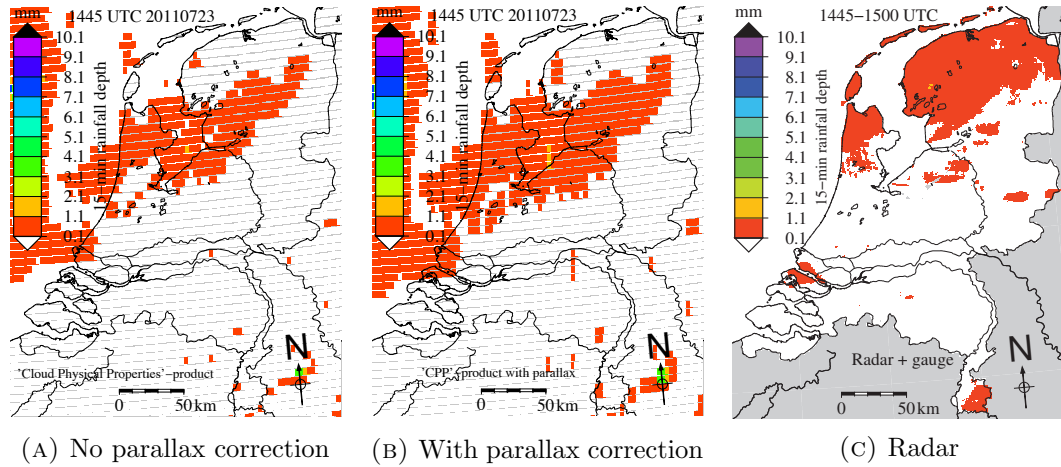


FIGURE 4.4: Cloud Physical Properties 15-minute rainfall depth (A) without and (B) with parallax correction compared to (C) gauge-adjusted radar data at 1445 UTC on 23 July 2011.

Day	False Alarm Ratio	Probability Of Detection	Accuracy
20 January	0.06	0.46	0.90
14 July	0.83	0.42	0.73
24 July	0.48	0.43	0.70
29 July	0.54	0.50	0.94

TABLE 4.4: Cloud Physical Properties performance of detecting wet and dry periods including the parallax correction.

Table 4.4 shows a reasonably low Probability of Detection and a high False Alarm Ratio. Only on 28 July 2011 the accuracy is high, which could be attributed to the low amount of precipitation that day. The satellite product will then also detect little precipitation and many pixels are correctly defined as dry.

As the probability of detecting precipitation would ideally be as high as possible, the same extension of the wet areas as was used for the Precipitating Clouds product is also applied to the Cloud Physical Properties product:

This improves the Probability Of Detection, which is a promising result, but also

Day	False Alarm Ratio	Probability Of Detection	Accuracy
20 January	0.30	0.83	0.91
14 July	0.86	0.69	0.54
24 July	0.54	0.62	0.65
29 July	0.76	0.91	0.82

TABLE 4.5: Performance of the Cloud Physical Properties product with the extension of the wet areas over 19 January, 13, 23 and 28 July 2011

the False Alarm Ratio increases and the accuracy decreases. As the improvement of the Probability Of Detection is much larger than the deterioration of the False Alarm Ratio and accuracy, the extension of the wet area is maintained in the rest of the research and

the Cloud Physical Properties product will be further tested for wet-dry classification. This is different from the threshold selection done for the Precipitating Clouds product as in that case the increasing Probability Of Detection and decreasing False Alarm Ratio with decreasing threshold height was trivial. The accuracy was therefore the best criterium for choosing a suitable threshold.

## 4.2 Raw link data

The interpolated rainfall maps calculated from the raw link data are shown only in terms of False Alarm Ratio, Probability Of Detection and accuracy as this is the best way to compare the results from the different wet-dry classifications to the situation without any wet-dry classification. Table 4.6 shows the statistics for the raw link data for the three summer days investigated in earlier sections as no winter data was available for the links.

The False Alarm Ratio is relatively high for both 13 and 28 July 2011. The reason

Day	False Alarm Ratio	Probability Of Detection	Accuracy
14 July	0.6	0.43	0.85
24 July	0.27	0.71	0.77
29 July	0.64	0.72	0.96

TABLE 4.6: The ability to detect wet and dry periods using raw link data without filter and wet-dry classification in terms of False Alarm Ratio, Probability Of Detection and accuracy.

that this ratio is low in the case of 23 July 2011 is that this day was very wet and therefore few dry pixels could be measured incorrectly as wet by the links. The Probability Of Detection is high, about 70%, without the use of any wet-dry classification for two of the three investigated days.

### 4.2.1 Combining Precipitating Clouds with raw link data

As the Precipitating Clouds product gave the best results in terms of Probability Of Detection when using the extended rainfall areas, this extended data set is used for wet-dry classification on the raw link data. The results are shown for one 15-minute period on 23 July 2011 in Figure 4.5 and the average for each day is given in table 4.7.

Although the large rainfall area is not totally detected by the combination of links and Precipitating Clouds product this is reflected in the link rainfall map by smaller wet regions. Other rainfall areas measured by the radar like the ones in the southern and eastern part of the Netherlands are (largely) not detected at all by the links combined with the Precipitating Clouds product. A better indication of the performance is

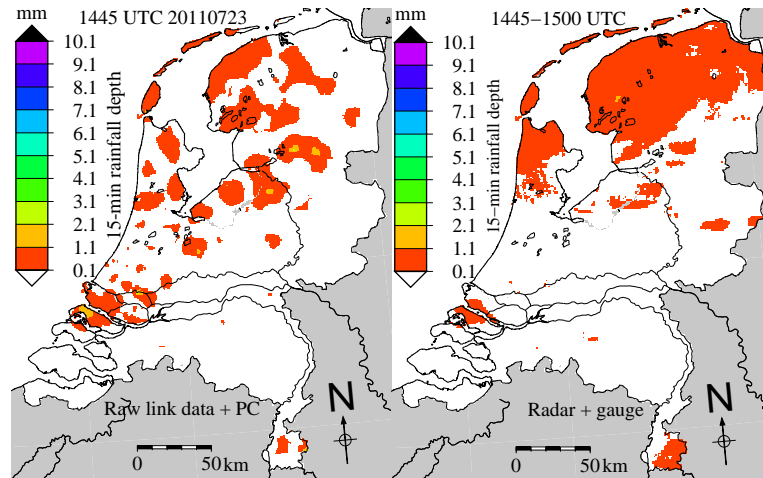


FIGURE 4.5: (*Left*) Link-based 15-minute rainfall depth using the Precipitating Clouds product with extended wet areas as wet-dry classification for the Netherlands, 1445 UTC on 23 July 2011. (*Right*) Gauge-adjusted radar 15-minute rainfall depth.

obtained by considering the ability of the link and Precipitating Clouds combination to detect wet and dry areas shown in Table 4.7.

Day	False Alarm Ratio	Probability Of Detection	Accuracy
14 July	0.41	0.35	0.89
24 July	0.22	0.66	0.78
29 July	0.44	0.58	0.98

TABLE 4.7: Precipitation Clouds statistics for an extended rainfall area used a a wet-dry classification on raw link data.

The use of the Precipitating Clouds product as a wet-dry classification gives a slight increase in the ability of the links to classify wet and dry areas. Comparing with the statistics for raw link data only (Table 4.6), the use of the Precipitating Clouds product shows obviously lower False Alarm Ratios, lower Probabilities Of Detection and slightly higher accuracies. Although the Probability Of Detection decreases, the decrease in False Alarm Ratio and slight increase in accuracy, which was already high, indicate already pretty good results. Still, the Probability Of Detection is too low to use only the Precipitating Clouds product as a wet-dry classification instead of no wet-dry classification.

Considering only the daytime situation, a better comparison can be made to the wet-dry classification using the Cloud Physical Properties product, which only is available during daytime. Table 4.8 shows the ability of the links to detect wet and dry areas using the Precipitating Clouds product with extended wet areas as wet-dry classification during daytime.

Day	False Alarm Ratio	Probability Of Detection	Accuracy
14 July	0.33	0.40	0.92
24 July	0.32	0.51	0.80
29 July	0.40	0.64	0.97

TABLE 4.8: Precipitation Clouds daytime statistics for an extended rainfall area used a wet-dry classification on raw link data.

Comparing the daytime statistics to the overall statistics of Precipitating Clouds as a wet-dry classification, whether or not the performance gets better when using just the daytime algorithm depends on the investigated day. In order to be able to make stronger statements a longer period has to be investigated.

#### 4.2.2 Combining Cloud Physical Properties with raw link data

As extending the rainfall areas gives better results in detecting precipitation than using only the parallax corrected data, the extended data set including the parallax correction is used as a wet-dry classification. When applying this data set of the Cloud Physical Properties product on the raw link data Figure 4.6 and Table 4.9 are obtained.

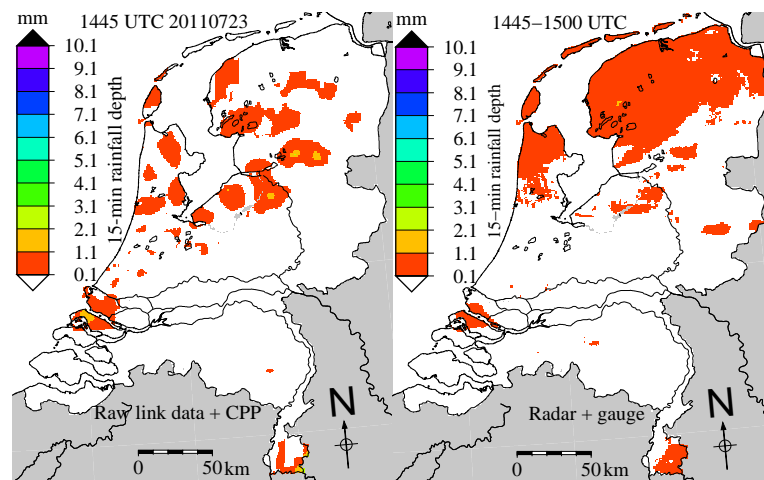


FIGURE 4.6: (Left) Link-based 15-minute rainfall depth using the Cloud Physical Properties product with extended wet areas as wet-dry classification for the Netherlands, 1445 UTC on 23 July 2011. (Right) Gauge-adjusted radar 15-minute rainfall depth.

Figure 4.6 shows that at least in this case the links using the Cloud Physical Properties product as wet-dry classification detects less of the radar-measured wet areas than for the Precipitating Clouds as wet-dry classification. Table 4.9 shows this happens not only in this case as the False Alarm Ratio is higher, the Probability Of Detection is lower for two of the three days and the accuracy is slightly lower compared to Table 4.8.



Since the Cloud Physical Properties product is only available during daytime, the

Day	False Alarm Ratio	Probability Of Detection	Accuracy
14 July	0.68	0.42	0.91
24 July	0.43	0.36	0.79
29 July	0.47	0.63	0.96

TABLE 4.9: Cloud Physical Properties statistics including a parallax correction and an extended area declared as wet. This extended data set is used a a wet-dry classification on raw link data.

results only reveal the daytime performance. When comparing to the statistics of only the raw link data, the accuracy increases for two of the three days while the Probability Of Detection decreases, especially for 23 and 28 July. Clearly too much of the wet pixels are filtered out of the data set by using the Cloud Physical Properties product. This can also be seen in the False Alarm Ratio for 13 and 28 July. Remarkable is that while the Probability Of Detection decreases for 28 July 2011, so does the False Alarm Ratio. Apparently more pixels incorrectly stated as wet are justly filtered out of the data set by the Cloud Physical Properties product than pixels which were correctly defined wet and therefore resulting in a lower False Alarm Ratio. Comparing the Cloud Physical Properties product to the daytime statistics of the Precipitating Clouds product, the satellite products give comparable results. The only difference is the higher False Alarm Ratio and for 21 July a lower Probability Of Detection in case of the Cloud Physical Properties product.

Using just the Cloud Physical Properties product as a wet-dry classification is not very useful compared to the raw link data and because of the fact that the satellite product is just usable during the day. In addition, for one of the three investigated days the False Alarm Ratio turned out to be much higher and the Probability Of Detection much lower compared to the performance of the raw link data. A combination of satellite products could possibly improve the results of the satellite approach.

### 4.3 Combining Precipitating Clouds and Cloud Physical Properties in wet-dry classification

When combining the Precipitating Clouds and Cloud Physical Properties products in the wet-dry classification the probability of detecting precipitation increases. This happens because a satellite pixel is defined as wet when at least one of the satellite products detects precipitation. During the day both satellite products are used but during the night only Precipitating Clouds is used as no Cloud Physical Properties data is available during this period. The result of combining the two satellite products is visualized in

Figure 4.7 for the same moment as was used in the previous sections.

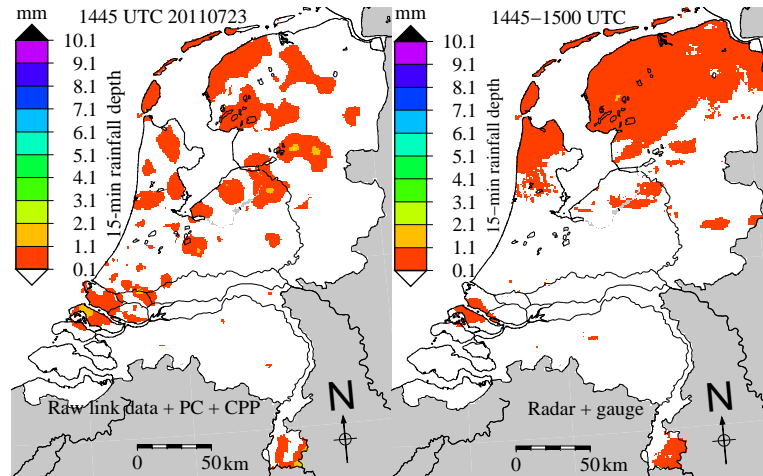


FIGURE 4.7: (*Left*) Link-based 15-minute rainfall depth using the combination of the Precipitating Clouds and Cloud Physical Properties products with extended wet areas as wet-dry classification for the Netherlands, 1445 UTC on 23 July 2011. (*Right*) Gauge-adjusted radar 15-minute rainfall depth.

All the wet areas which were seen on the left hand side of Figures 4.5 and 4.6 are combined in Figure 4.7, increasing the chance that precipitation is detected, but also possibly increasing the amount of false alarms. The performance of the combined wet-dry classification is shown in Table 4.10.

Day	False Alarm Ratio	Probability Of Detection	Accuracy
14 July	0.53	0.39	0.87
24 July	0.24	0.68	0.78
29 July	0.47	0.67	0.95

TABLE 4.10: Statistics for a wet-dry classification using Precipitating Clouds and Cloud Physical Properties data combined with link data.

For both 23 July and 28 July 2011 the Probability Of Detection is larger than the Probability Of Detection of the separate satellite products applied on the raw link data, which was expected. This is not the case for 13 July 2011, where the Probability Of Detection is higher than when only the Precipitating Clouds product is applied to the raw link data, but smaller than when applying just the Cloud Physical Properties product as a wet-dry classification on the raw link data. This can be explained by the fact that the Cloud Physical Properties product is only available when the sun zenith angle is smaller than  $78^\circ$ , which is during the day. The Precipitating Clouds Product and the combination of Precipitating Clouds and Cloud Physical Properties as a wet-dry

classification is available during both day and night. When combining the two satellite products, during the night only the Precipitating Clouds data is used and the amount of time over which the Probability Of Detection is determined is larger when looking at the combination of the two products than when considering only the Cloud Physical Properties product.

Compared to the raw link data, the accuracy slightly increases for two days, but the Probability Of Detection slightly decreases and the False Alarm Ratio decreases for all cases. For classifying wet and dry areas the raw link data appears to give slightly better results. However, as the received link signal level also fluctuates during dry weather, a wet-dry classification using the Precipitating Clouds and Cloud Physical Properties product could be useful for improving link-based rainfall depth estimations.

## 4.4 Adding the combined wet-dry classification to the program

### 4.4.1 Without filter

When using the combination of the Precipitating Clouds and Cloud Physical Properties products for the satellite approach without filter, the optimal parameter values  $A_a=2.4$  dB and  $\alpha=0.245$  are found. Applying these to the 12 days of the validation set results in the daily accumulated rainfall depths for the satellite approach shown in Figures 4.8 and 4.9. The number of links used for the satellite approach without filter is the same as was used for the raw link rainfall maps as no links were removed by a filter. In order to see the effect of applying the satellite approach, Figures 4.8 and 4.9 show also the daily accumulated rainfall depths without any wet-dry classification or filter. Optimal parameter values found for this raw link data are  $A_a=2.4$  dB and  $\alpha=0.27$ . These optimal values indicate that the correction for wet antennas is the same for both cases (with and without satellite approach), but for the satellite approach the maximum specific attenuation  $k_{max}$  gives a slightly smaller contribution to the path-averaged rainfall intensity  $\langle R \rangle$ . This compensates for incorrectly filtered wet pixels.

The raw link data without any wet-dry classification showed to give good results in terms of classifying wet and dry areas. Figures 4.8 and 4.9 show the daily rainfall maps calculated using, from left to right, the raw link data, satellite approach, radar approach (the best performing approach without filter) and the radar-based rainfall maps (the ground truth). For the daily rainfall maps a pixel is dry if the rainfall depth is smaller than 1 mm. Overall, the rainfall maps using the radar approach resemble

the radar-based rainfall maps most but the raw link data maps also show the large features of the wet areas seen in the radar data reflected in the link rainfall maps, but using the satellite approach improves these results. Part of the outliers seen in the raw link data are correctly reduced as can be seen especially for 11 June, 9 August and 11 September 2011. Furthermore, areas shown by the raw link data as wet while it should be dry according to the radar are correctly reduced by the satellite approach as can be seen on for example 26 August 2011. This is because by (incorrectly) removing a part of the dry areas when using the satellite approach the optimal parameter value for  $\alpha$  decreased, resulting in a larger contribution of  $k_{min}$  to the path-averaged rainfall depth  $\langle R \rangle$  (equation 2.6). The rainfall intensities decrease and more links are labeled dry. When interpolating the path averaged rainfall depths more areas will show as dry in the rainfall maps. The opposite is also seen in the Figures: areas which should be wet according to the radar data but shown as dry by the raw link data, correctly show more precipitation with use of the satellite approach. This can be caused by a higher reference level for the link approach as this is not calculated over both wet and dry periods anymore. With a higher reference level, the specific attenuation increases, resulting in a higher path averaged rainfall intensity. When interpolating these rainfall intensities to the radar grid, the resulting rainfall map shows more wet areas.

The results shown in Figures 4.8 and 4.9 are promising but in order to get a more detailed insight in the performance of the satellite approach, Figures 4.10 and 4.11 show scatter plots for respectively 15 minute rainfall maps with a resolution of 81 km<sup>2</sup> and daily rainfall maps with a resolution of 1 km<sup>2</sup>.

The raw link data and the satellite approach show an underestimation of the mean 15-minute rainfall depth, about 4.7% for the raw link data and 17.4% for the satellite approach. This is also seen in the scatter plot where most of the points are located on the right hand side of the diagonal, although the difference in performance between no wet-dry classification and the satellite approach is reflected more clearly in the values of  $CV$  and  $\rho^2$ .

Although the underestimation is larger for the satellite approach,  $CV$  is lower and  $\rho^2$  is higher for the satellite approach. The coefficient of variation  $CV$  decreases to 1.14 when using a wet-dry classification, indicating that the link data varies less from the radar data than when no wet-dry classification is used. The correlation coefficient  $\rho^2$  has increased to 0.41, indicating an increased positive correlation and agreement between the link and radar data.

According to the scatter plots in Figure 4.11, the daily rainfall depths show a slight overestimation of about 0.46% when no wet-dry classification is used, while the satellite

approach still shows an underestimation of about 14.7%. Quite some outliers are present at the top of both scatter plots. Especially for the raw link data, the largest rainfall depths overestimate the real amount of precipitation. Using the satellite approach reduces part of these outliers. As there are still a large amount of outliers present, this shows the possible need for a filter which removes these outliers even further.

Table 4.11 shows a summary of the performances of the raw link data, satellite approach and radar approach without filter.  $\bar{R}_{radar}$  and  $\bar{R}_{link}$  are calculating from those rainfall depths where the links and/or radar have measured more than 0.1 mm. Looking at the daily rainfall depths, the satellite approach causes  $CV$  to decrease to 0.75 with respect to the raw link data, while  $\rho^2$  increases to 0.49. When accumulating the 15-minute rainfall depths to obtain daily rainfall depths, the improvements in  $CV$  and  $\rho^2$  also grow larger. This can be a result of using accumulated values but also by increasing the resolution from 81 km<sup>2</sup> to 1 km<sup>2</sup> reducing the influence of outliers as they will affect a much smaller area. The radar approach perform best when no filter is used. This is reflected in Table 4.11 by the lower  $CV$  and higher  $\rho^2$  compared to the satellite approach.

	$\bar{R}_{radar}$	$\bar{R}_{link}$	$CV$	$\rho^2$
Raw link data (15 min)	0.43	0.41	1.35	0.36
Satellite approach (15 min)	0.46	0.38	1.14	0.41
Radar approach (15 min)	0.47	0.44	1.12	0.47
Raw link data (daily)	8.62	8.66	1.15	0.30
Satellite approach (daily)	8.70	7.42	0.75	0.49
Radar approach (daily)	8.77	8.27	0.57	0.65

TABLE 4.11: Performance for raw link data, satellite approach and radar approach without filter

In addition, the statistics used in the previous sections are also calculated for the satellite approach and the raw link data. The raw link data gives a False Alarm Ratio of 0.38, a Probability Of Detection of 0.64 and an accuracy of 0.89. The satellite approach gives a False Alarm Ration of 0.31, a Probability Of Detection of 0.62 and an accuracy of 0.90. These differ not much from each other except for the False Alarm Ratio, which decreases from 0.38 to 0.31 when the satellite approach is used as a wet-dry classification. This makes sense as the satellite approach removes attenuations not related to precipitation (according to the satellite products), decreasing the fraction of false alarms in the final results.

#### 4.4.2 With filter

Applying the -130 dB filter would probably improve the results even more. The optimal parameter values change to  $A_a=2.7$  dB and  $\alpha=0.29$  when using the filter. Figures 4.12

and 4.13 show the daily accumulations for the satellite approach with filter compared to raw link data with filter, the link approach with filter (the best performing approach) and radar-based rainfall maps.

The use of a filter clearly removes or reduces some of the large rainfall depths given by the satellite approach, showing a better resemblance to the radar data. The link data still underestimates the real precipitation, but this was expected as only the outliers are removed by the filters. Overall, the filter improves the results from the link data. Figure 4.14 shows the scatter plot of the daily rainfall maps for the satellite approach with filter.

	$\bar{R}_{radar}$	$\bar{R}_{link}$	$CV$	$\rho^2$
Raw link data (15 min)	0.44	0.41	1.18	0.45
Satellite approach (15 min)	0.47	0.39	1.09	0.46
Link approach (15 min)	0.46	0.45	1.13	0.49
Raw link data (daily)	8.64	8.34	0.64	0.59
Satellite approach (daily)	8.72	7.45	0.52	0.68
Link approach (daily)	8.75	8.91	0.53	0.73

TABLE 4.12: Performance for raw link data, satellite approach and link approach with filter

The underestimation remains similar compared to the satellite approach without filter as using the filter reduces the rainfall depths by removing outliers and giving a larger optimal value for  $A_a$ , which will correct more strongly for wet antennas, while an increase in the optimal value of  $\alpha$  increases the rainfall depths by  $k_{max}$  having a larger contribution to the path-averaged rainfall intensity. The resulting increases and decreases in rainfall depth point out to be comparable, resulting in a similar underestimation as was found for the satellite approach without filter.  $CV$  and  $\rho^2$  clearly improve. This is because the outliers are not interpolated, or less than without using the filter and the deviation of the link data from radar data is reduced. The scatter plot clearly shows the effect of the filter by a reduction of the number of data points in the top left corner.

This improvement is not reflected in all statistics: when applying the filter to the raw link data, this gives a False Alarm Ratio of 0.32, a Probability Of Detection of 0.61 and an accuracy of 0.90, which is comparable to the results without use of the filter.

However, from the comparison of the 12 daily rainfall maps and scatter plots with accompanying statistics for the satellite approach with and without filter, the conclusion can be drawn that the use of a filter greatly improves the results from the satellite approach.

### 4.4.3 Comparison to the radar and link approach

#### 4.4.3.1 No filter

Figure 4.15 shows the daily rainfall map scatter plots for the different wet-dry classifications without filter. Although the satellite approach shows promising results when comparing to the raw link data, the radar approach still gives better results when looking at the statistics shown in Figure 4.15. A summation of these values for all wet-dry classifications is also shown in Table 4.13.

Larger differences are found in the statistics from Table 4.13. Using a wet-dry classification certainly improves the values of  $CV$  and  $\rho^2$ . This proves that the use of a wet-dry classification is desired when making link-based rainfall estimations. Compared to the link and radar approaches, the satellite approach does not give bad results but the radar approach clearly performs better.

The performance in terms of the False Alarm Ratio, Probability Of Detection and accuracy is not shown in this thesis but this turned out to be comparable for the three different approaches, however the radar approach performs somewhat better than the satellite approach.

	$\bar{R}_{radar}$	$\bar{R}_{link}$	$CV$	$\rho^2$
Raw link data	8.62	8.66	1.15	0.3
Satellite approach	8.70	7.42	0.75	0.49
Link approach	8.79	7.17	0.57	0.62
Radar approach	8.77	8.27	0.57	0.65

TABLE 4.13: Performance for daily rainfall depths of raw link data and the different wet-dry classifications without filter

#### 4.4.3.2 Filter

As the results of the satellite approach greatly improved by applying the filter, all wet-dry classifications are regarded with filter. Figure 4.16 shows the scatter plots for the daily rainfall depth of the link and radar approaches with filter. Looking at the scatterplots, no large differences can be seen so the best way to compare the different approaches is by looking at the statistics shown in Tables 4.14 and 4.15.

It is clear from Tables 4.14) and 4.15 that even when the filter is applied to the raw link data, wet-dry classification greatly improves results in terms of a decreasing False

Alarm Ratio, increasing Probability Of Detection (for the link and radar approaches), decreasing  $CV$  and increasing  $\rho^2$ .

	False Alarm Ratio	Probability Of Detection	Accuracy
Raw link data	0.37	0.63	0.89
Satellite approach	0.32	0.61	0.90
Link approach	0.32	0.67	0.91
Radar approach	0.32	0.72	0.91

TABLE 4.14: False Alarm Ratio, Probability Of Detection an accuracy given by the different wet-dry classifications with filter.

	$\bar{R}_{radar}$	$\bar{R}_{link}$	$CV$	$\rho^2$
Raw link data	8.64	8.34	0.64	0.59
Satellite approach	8.72	7.45	0.52	0.68
Link approach	8.75	8.91	0.53	0.73
Radar approach	8.74	9.82	0.55	0.74

TABLE 4.15: Statistics for daily rainfall depths of raw link data and the different wet-dry classifications with filter

When using a filter, the performance of the satellite approach is comparable to the link and radar approaches but the other approaches perform better in terms of Probability Of Detection (Table 4.14). Table 4.15 also shows that the satellite approach gives good results compared to the other approaches, but when possible the link or radar approach can still be used best as their bias and  $\rho^2$  are respectively lower and higher than for the satellite approach.



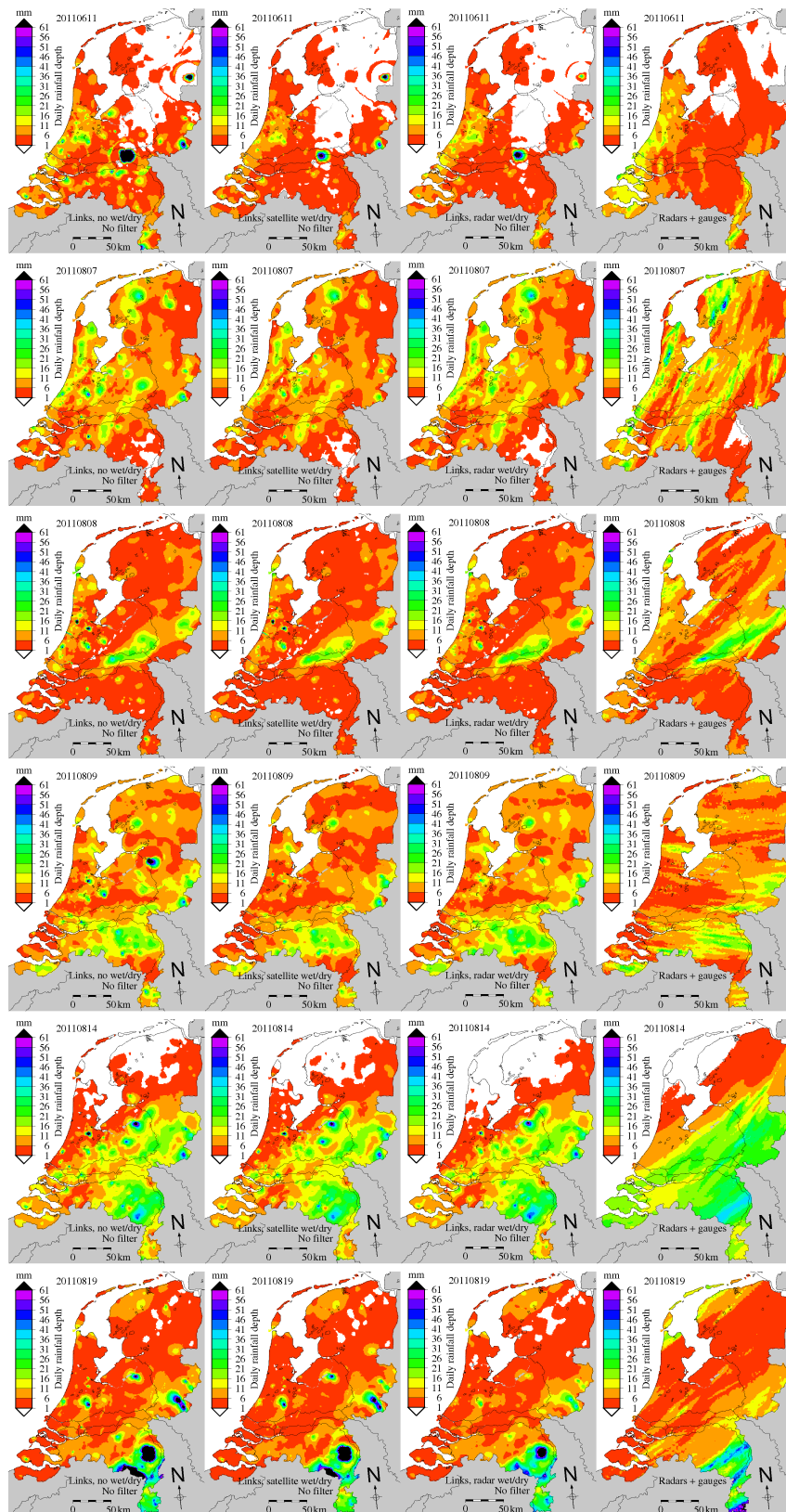


FIGURE 4.8: Daily link-based rainfall maps for the first 6 days of the validation set (four panels each) compared to radar-based rainfall maps. (*First panel*) No wet-dry classification. (*Second panel*) Satellite approach. (*Third panel*) Radar approach. (*Fourth panel*) Gauge-adjusted radar ('ground-truth').

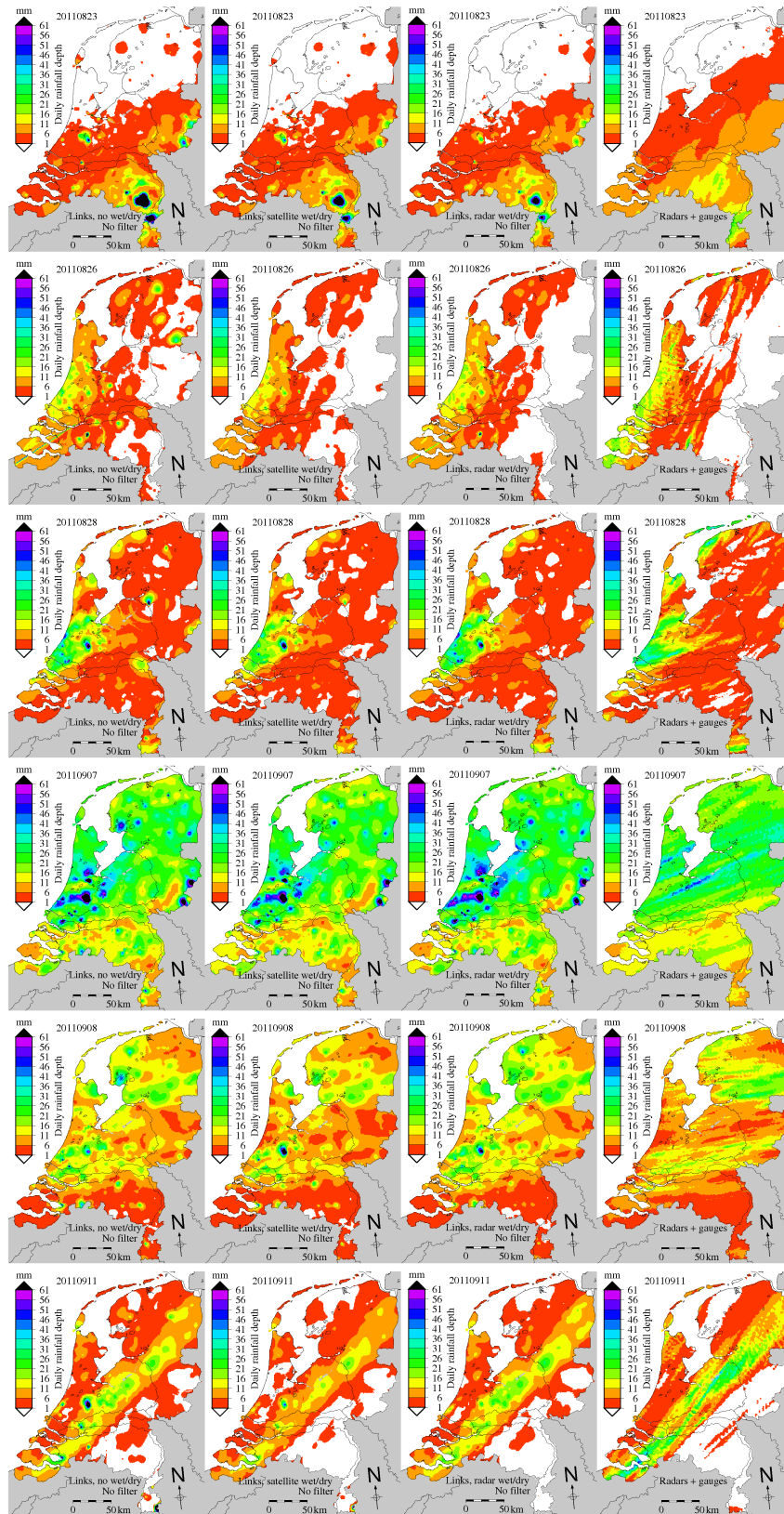
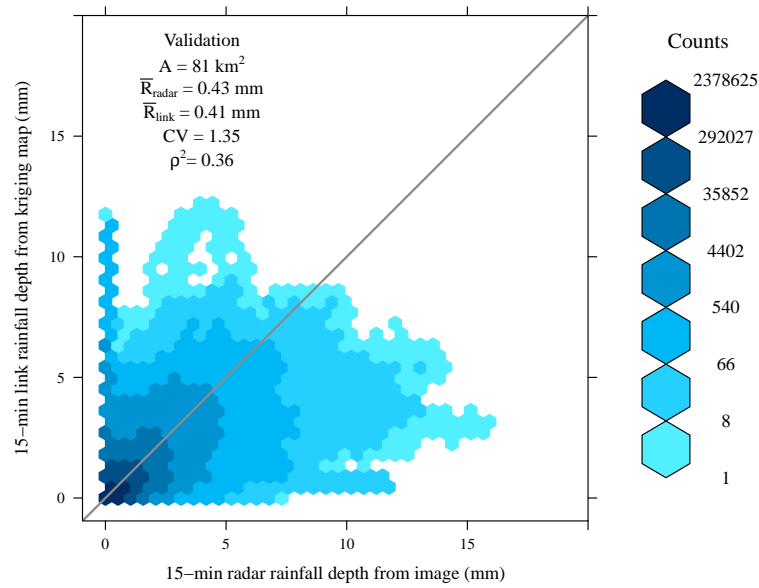
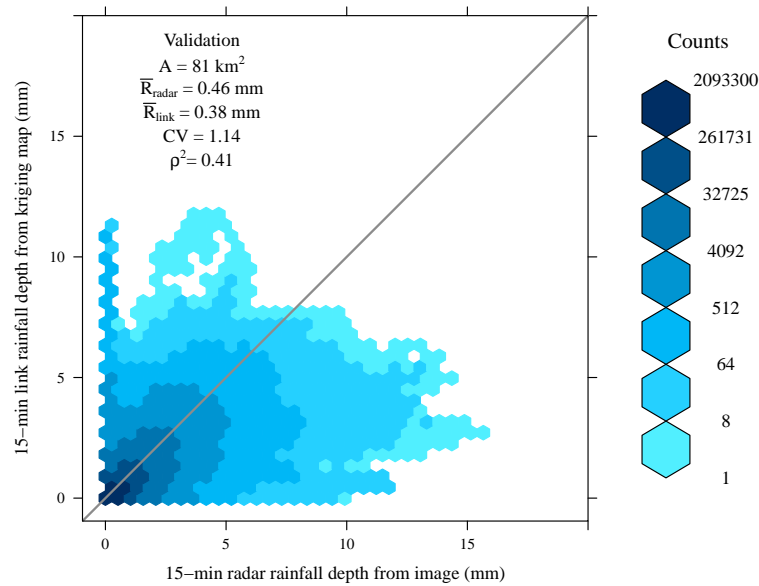


FIGURE 4.9: Daily link-based rainfall maps for the last 6 days of the validation set (four panels each) compared to radar-based rainfall maps. (*First panel*) No wet-dry classification. (*Second panel*) Satellite approach. (*Third panel*) Radar approach. (*Fourth panel*) Gauge-adjusted radar (ground truth).

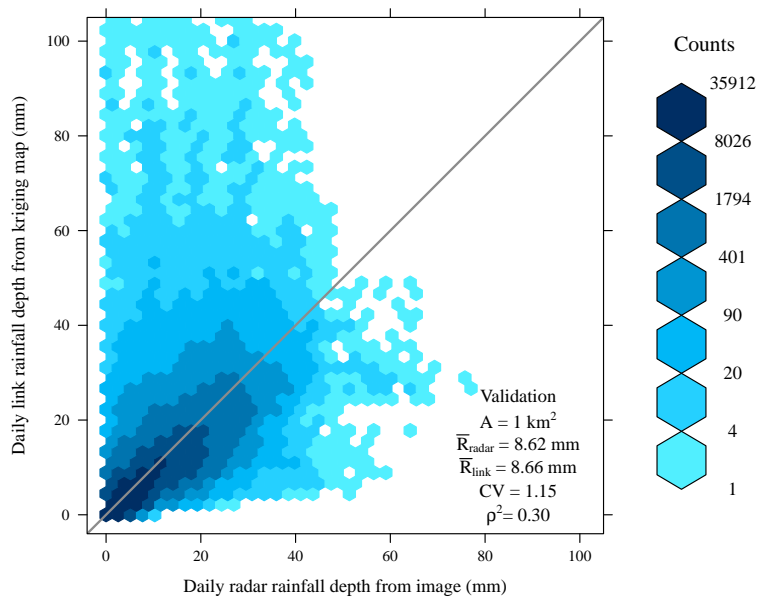


(A) Raw link data without wet-dry classification

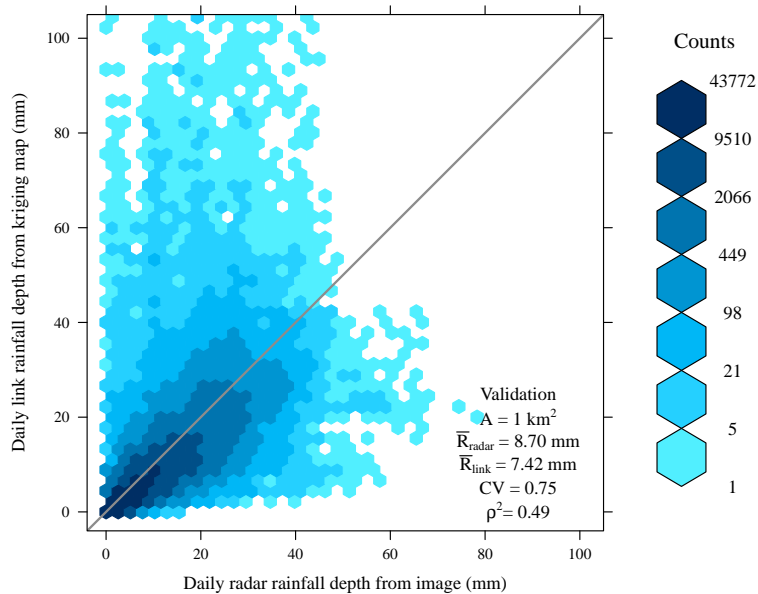


(B) Satellite approach

FIGURE 4.10: Validation of 15-minute link rainfall maps against radar rainfall maps for an area size  $A$  of  $81 \text{ km}^2$ . The gray line is the  $y = x$  line,  $\bar{R}$  denotes the average rainfall depth at the radar pixel,  $CV$  is the coefficient of variation and  $\rho^2$  is the coefficient of determination. Only those rainfall depths are used where the link and/or radar have measured more than  $0.1 \text{ mm}$ . (A) Validation of link rainfall maps without applying any wet-dry classification or filter. (B) Validation of link rainfall maps using the satellite approach without filter.



(A) No wet-dry classification



(B) Satellite approach

FIGURE 4.11: Validation of daily link rainfall maps against radar rainfall maps for each radar pixel of  $1 \text{ km}^2$ . (A) Validation of link rainfall maps without applying any wet-dry classification or filter. (B) Validation of link rainfall maps using the satellite approach without filter.

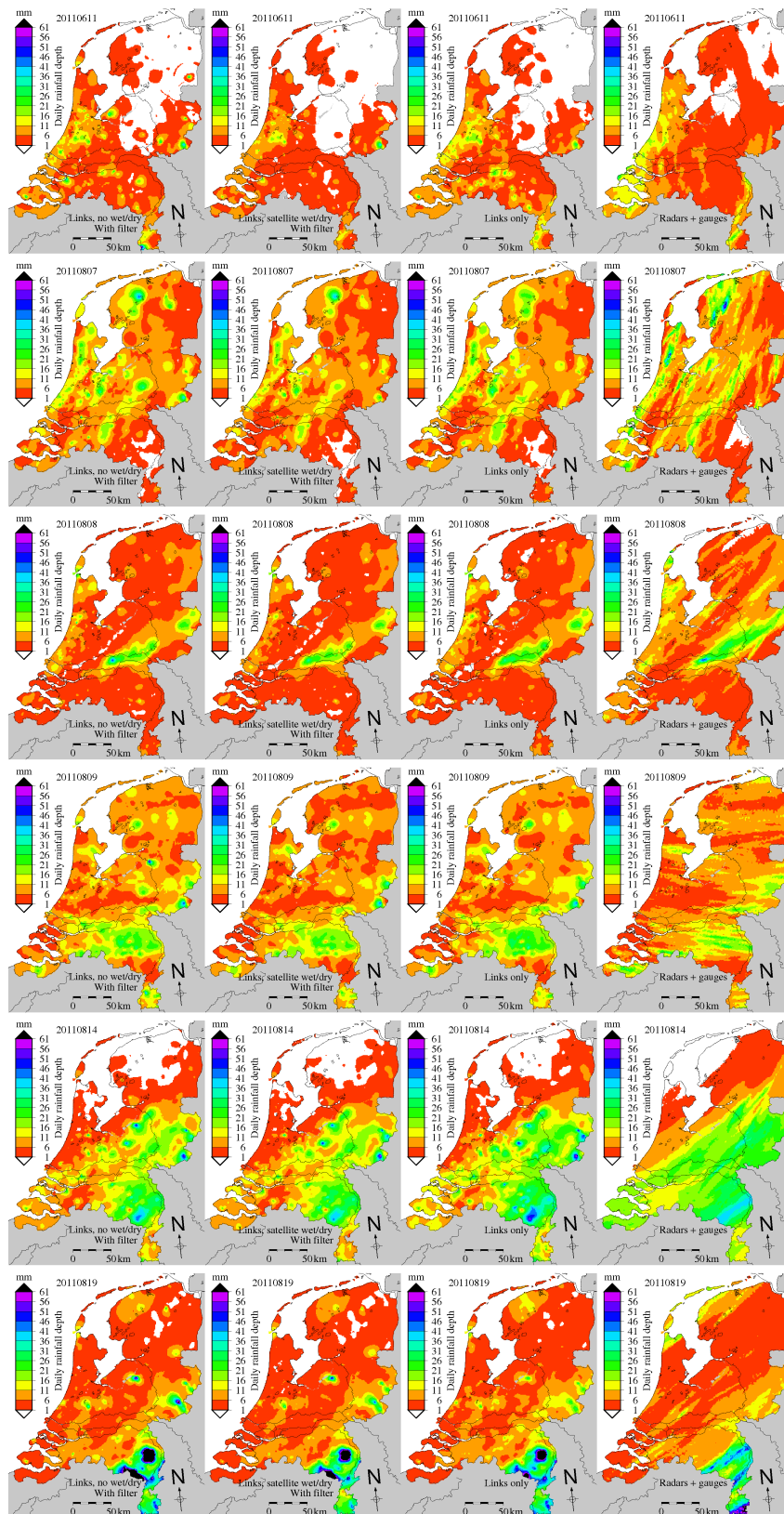


FIGURE 4.12: Daily link-based rainfall maps for the first 6 days of the validation set (four panels each) compared to radar-based rainfall maps. (*First panel*) No wet-dry classification with filter. (*Second panel*) Satellite approach with filter. (*Third panel*) Link approach with filter. (*Fourth panel*) Gauge-adjusted radar (ground truth).

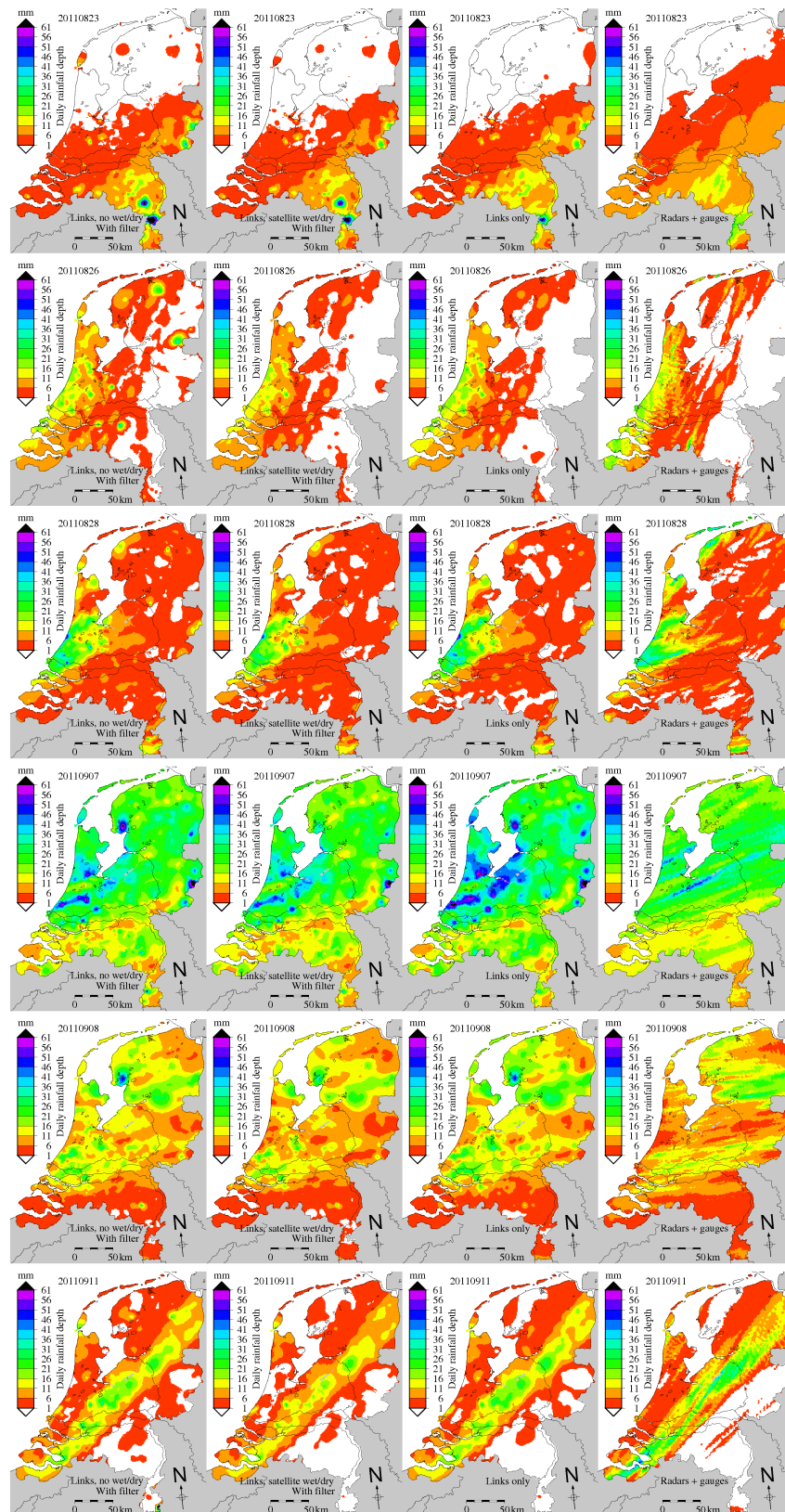


FIGURE 4.13: Daily link-based rainfall maps for the last 6 days of the validation set (four panels each) compared to radar-based rainfall maps. (*First panel*) No wet-dry classification with filter. (*Second panel*) Satellite approach with filter. (*Third panel*) Link approach with filter. (*Fourth panel*) Gauge-adjusted radar (ground truth).

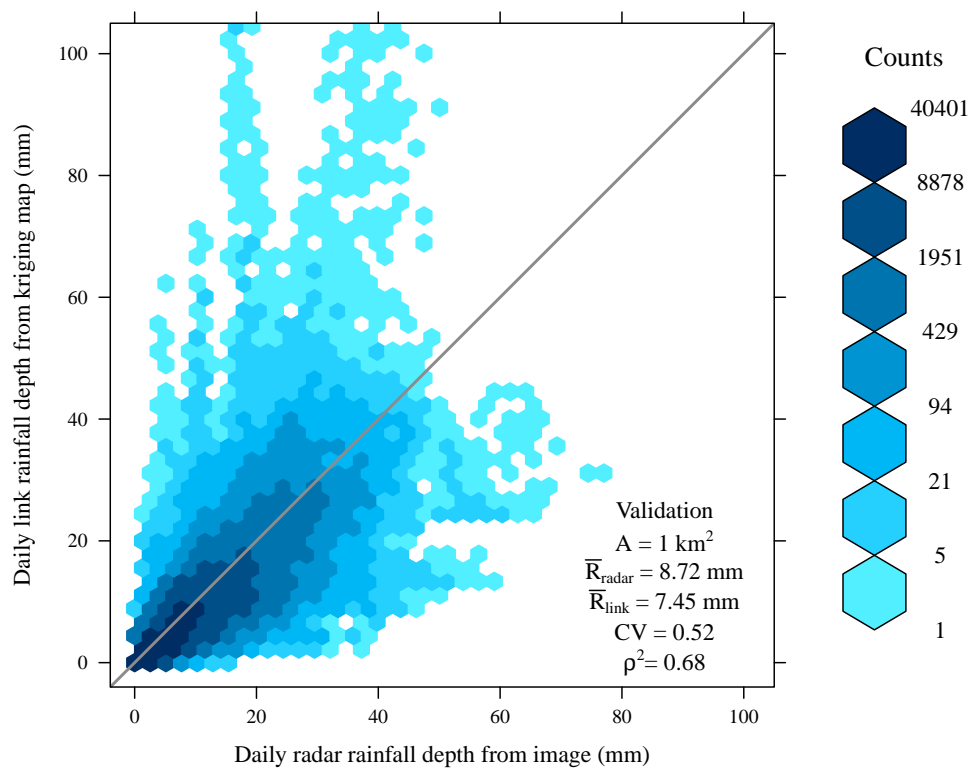
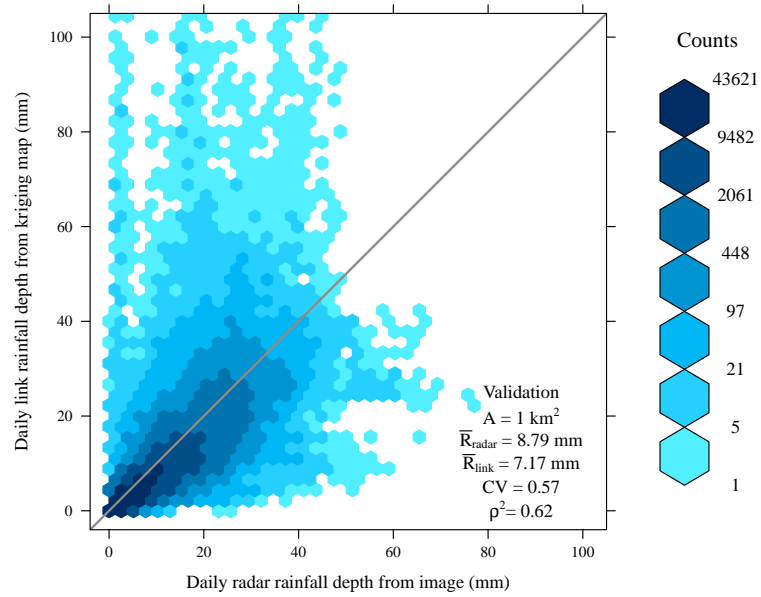
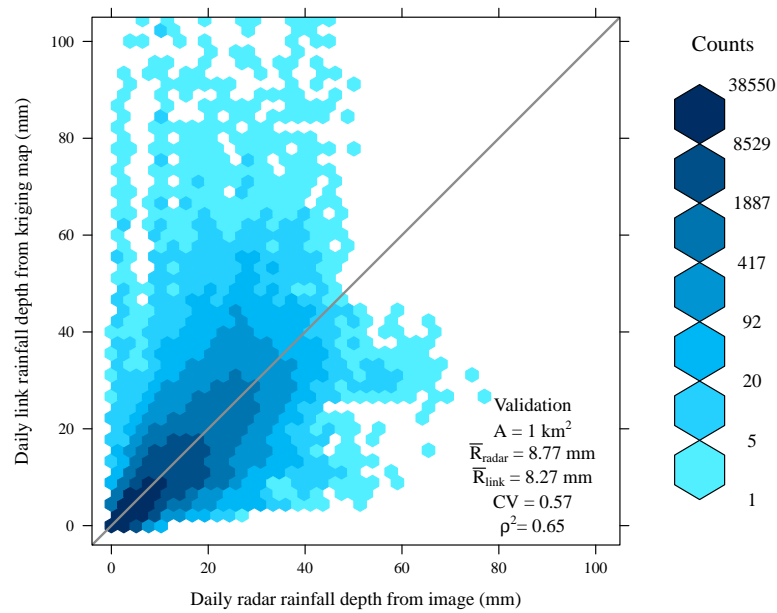


FIGURE 4.14: Validation of daily link rainfall maps using the satellite approach with filter against radar rainfall maps for each radar pixel of  $1 \text{ km}^2$ .



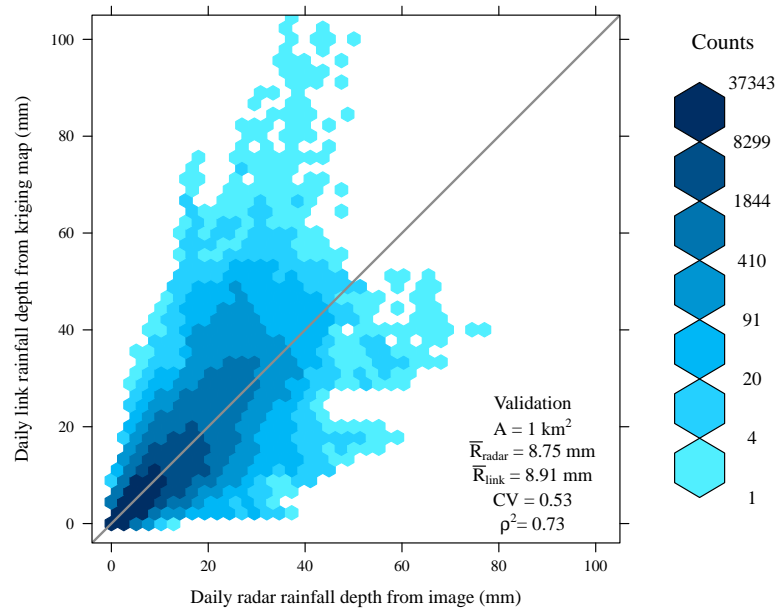
(A) Link approach



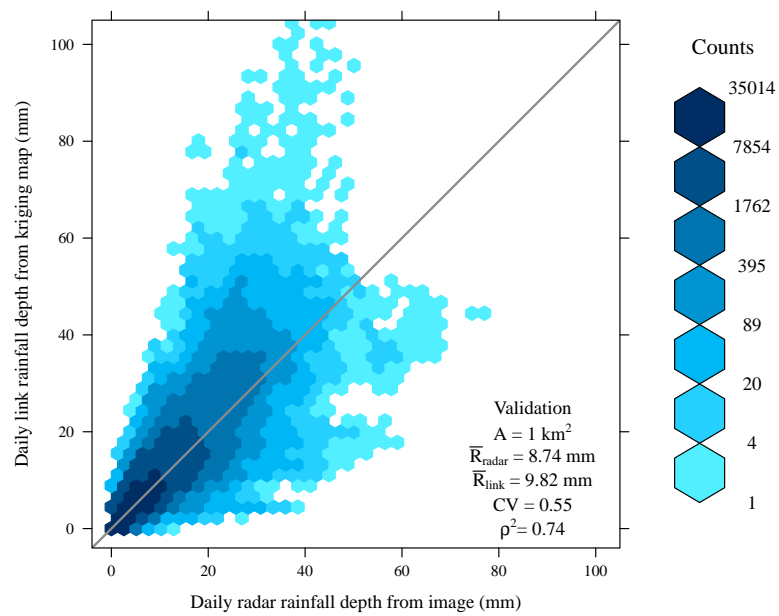
(B) Radar approach

FIGURE 4.15: Validation of daily link rainfall maps against radar rainfall maps for each radar pixel of  $1 \text{ km}^2$ . (A) Validation of the link approach without filter. (B) Validation of the radar approach without filter.





(A) Link approach



(B) Radar approach

FIGURE 4.16: Validation of daily link rainfall maps against radar rainfall maps for each radar pixel of  $1 \text{ km}^2$ . (A) Validation of the link approach with filter. (B) Validation of the radar approach with filter.

## Chapter 5

# Discussion

Aim of this thesis was to develop a satellite based wet-dry classification for measuring rainfall using microwave links and investigate whether this approach could be used as an alternative for the existing link and radar approaches. The satellite approach showed good results, having a quality almost as high as the radar and link approaches when using a filter. The optimized parameter values of  $A_a$  and  $\alpha$  also do not differ much between the different approaches. These are very promising results. Without use of the filter, the performance of the satellite approach is clearly lower than for the radar and link approaches without filter and is therefore no good alternative for the existing wet-dry classifications. It is important to note that this holds for the Dutch link network.

The best results for the satellite approach were gained by using the filter but in order to apply the filter, a sufficiently dense microwave link network has to be present and part of the link approach has to be used. A network is sufficiently dense if for each link at least 3 other links are available in a 15 km radius. This would mean that whenever the filter can be applied, the link approach can be used in the precipitation measurements, which performs better than the satellite approach at this point assuming the link approach thresholds perform correctly. For other networks than the one used in this thesis these thresholds possibly need adjustments.

Link-based precipitation measurements can only be done correctly for rainfall. Solid precipitation can not be measured as is described in [Vivekanandan et al. \[1999\]](#). Melting solid precipitation can be measured but as the properties are different from those of rain, the link signal is attenuated in a different way resulting in incorrect precipitation intensities when using the method applied in this thesis. When considering the rainfall measurements the obtained rainfall intensities from the links are path-averaged. This will have a small effect for the short links, but for longer links this average value can not always correctly represent the situation over the whole link. For areas with a high link density as cities this will not be a real problem but in rural areas this will result in less

detailed rainfall information in terms of spatial variation. The difference in link density will also likely result in less links to be rejected for the cities than for the rural areas when using the link approach as more links are available in a 15 km radius for urban areas.

A limitation for applying the satellite approach, or any of the other approaches, in other countries is the dependency on the availability of radar or rain gauge data. After all, the optimization of  $A_a$  and  $\alpha$  depends on the comparison of the calibration link data with the radar (and/or rain gauge) data, which is assumed to represent the ground truth. When no radar or rain gauge data are available, no optimization can be done using the method used in this thesis. The Dutch values for  $A_a$  and  $\alpha$  can be used as a first approximation. When considering a country with a similar climate as for the Netherlands these values can be maintained. Another possibility is to set up a measurement campaign for acquiring rain gauge data for the period covered by the calibration data set. As was also said for the availability of a sufficiently dense link network, when radar data is available, using the radar approach is preferred over the satellite approach.

Because of the points mentioned above, it is hard to compare the different wet-dry classifications as all classifications depend on radar data for optimization and when using the filter also on the requirement of a sufficiently dense link network using part of the link approach. When using the results of the optimized routine, implying the availability of a radar and/or rain gauge network, probably the best way to compare the different approaches is by using the satellite approach without filter, the link approach with filter and the radar approach without filter as these can be applied independently and are therefore the most genuinely applicable. In other words, in this way the satellite and radar approaches are not dependent on (a part of) the link approach.

The satellite approach could be improved further as the satellite data can be used to detect and (temporarily) remove links which show a too large attenuation from the data set. A possible way to do this is to look at the link signals in the area classified as dry by the satellite. When a link in a dry area provides an attenuation larger than a stated threshold for multiple time steps, this link can be left out for, for example, half an hour or an hour. This will be most effective if the link is removed for a wet period as a link which gives a large attenuation for a dry period will likely also cause a high overestimation of precipitation during a wet period.

Another way to improve the satellite approach is by improving the detection of precipitation by the satellite products. Using more radiation channels can possibly be used to gather information of more cloud (and precipitation) properties or more information of already investigated cloud properties which could lead to a more accurate precipitation detection. Such an improvement in satellite products will likely be reflected in better results for the satellite approach.

Using multiple types of satellites could also improve results. When adding polar

satellites to the satellite approach to complement the geostationary satellite data for the periods for which polar satellite data is available, the quality of the wet-dry classification could improve. While a precipitation radar is not possible to use on a geostationary satellite because of the height of the orbit, polar satellites can make radar measurements as they are in a lower orbit, giving not only indirect but also direct rainfall observations [trm]. Combining these methods can improve the wet-dry classification using satellites for at least part of the investigated period.

Satellites have also some disadvantages. By measuring rainfall indirectly the obtained rainfall intensities can contain larger uncertainties than when using direct observations. Another disadvantage is that the temporal resolution is limited as large areas have to be measured. Measurements can not be done for the whole area at once so all satellites have a revisiting time resulting in a lower temporal resolution than for radar and rain gauges. In case of the Meteosat Second Generation satellite, for each 15-minute interval one measurement is done.

The gauge-adjusted radar data is used as ground-truth but this can still deviate from reality by for example evaporation of rain below the cloud base. Using rain-gauge data a correction is made for this effect but this is only an approximation and no complete correction.

## Chapter 6

# Conclusions

Continuing on the research done by [Overeem et al. \[2013\]](#), a new method is developed which uses satellites for classifying wet and dry periods as part of rainfall measurements employing a commercial cellular communication network. This new method can be used for areas where no weather radar or rain gauges are available for rainfall measurements. Unlike radar and rain gauges, satellites have an almost world wide coverage. In order to investigate the performance of a satellite-based wet-dry classification compared to the existing link and radar approaches, the same period, investigating area and rainfall calculations are used as described in [Overeem et al. \[2013\]](#). After calibrating with gauge-adjusted radar data for a 12-day calibration data set the method is validated using a 12-day validation data set. The calibration and validation sets both contain 12 (different) days from the period June-September 2011. The employed cellular communication network covering the Netherlands contains 2400 links with frequencies of 13-40 GHz.

For selecting useful satellite products from the geostationary Meteosat Second Generation satellite, 1 day in January 2011 and 3 days in July 2011 have been investigated for the Netherlands. This is done by comparing the detected wet and dry periods by the satellite products to a gauge-adjusted radar data set in terms of maps and False Alarm Ratio, Probability Of Detection and accuracy.

From the three studied satellite products, the Convective Rainfall Rate product detected not enough precipitation in order to use this product in a wet-dry classification. The Precipitating Clouds and parallax corrected Cloud Physical Properties products showed better results and can possibly be applied as a wet-dry classification. The Precipitating Clouds products performs best when a threshold of 20% is used for the presence of precipitation. After applying an extension of the wet areas by one satellite pixel, the Probability Of Detection improved greatly for both satellite products which favors the use of an extended wet area in the wet-dry classification based on the three investigated days.

While the separate products did not have a large Probability Of Detection, combining the two satellite products improved the Probability Of Detection as the wet areas are combined in one data set. Because of this the combination of the Precipitating Clouds and Cloud Physical Properties products is used in the satellite based wet-dry classification.

After optimizing the parameter values of  $A_a$  and  $\alpha$  using the 12-day calibration data set, the 15-minute and daily rainfall maps of the 12-day validation data set measured by only the raw link data without use of a wet-dry classification or filter to remove outliers already showed some promising resemblances to the radar data for the validation set. Using the satellite approach consisting of the combination of the Precipitating Clouds and Cloud Physical Properties products clearly showed even more improvements in terms of both the rainfall depths and the statistics. Applying the filter removed part of the outliers which had a positive effect on the results.

Comparison to the link and radar approaches showed that when no filter is used both radar and link approach clearly perform better than the satellite approach. The wet-dry classification using satellites does improve the results from the raw link data showing the need of a wet-dry classification. When the filter is used, the satellite approach performance is close to the link and radar approaches, although both the link and radar approach still perform better. Nevertheless, the satellite approach could be a useful alternative when the link and radar approach can not be applied.

From these results it can be concluded that satellites can successfully be used as a wet-dry classification for measuring rainfall employing a commercial cellular communication network. When using the filter, the satellite approach can be a very promising alternative to the existing link and radar approaches. Without the filter, the other approaches clearly perform better.

# Bibliography

- H. Messer, A. Zinevich, and P. Alpert. Environmental monitoring by wireless communication networks. *Science*, 312(5774):713, May 2006.
- H. Leijnse, R. Uijlenhoet, and J.N.M. Stricker. Rainfall measurement using radio links from cellular communication networks. *Water Resources Research*, 43, 2007.
- A. Zinevich, H. Messer, and P. Alpert. Frontal rainfall observation by a commercial microwave communication network. *Journal of Applied Meteorology and Climatology*, 48:1317–1334, 2009.
- A. Overeem, H. Leijnse, and R. Uijlenhoet. Country-wide rainfall maps from cellular communication networks. *Proc. Nat. Acad. Sciences*, 110:2741–2745, 2013.
- A. Overeem, H. Leijnse, and R. Uijlenhoet. Measuring urban rainfall using microwave links from commercial cellular communication networks. *Water Resources Research*, 47, 2011.
- G. Summer. *Precipitation. Process and Analysis*. John Wiley & Sons, Bath, 1988.
- M.F.P. Bierkens, A.J. Dolman, and P.A. Troch. *Climate and the hydrology cycle*. IAHS, 2008.
- J.R. Holton. *An introduction to dynamical meteorology*. Elsevier, 2004.
- URL <http://www.kennislink.nl>.
- H. Leijnse, R. Uijlenhoet, and J.N.M. Stricker. Microwave link rainfall estimation: Effects of link length and frequency, temporal sampling, power resolution, and wet antenna attenuation. *Advances in Water Resources*, 31:1481–1493, 2009.
- A. Overeem. Introductory lecture: Cloud formation and precipitation.
- R.A. Roebeling and I. Holleman. Seviri rainfall retrieval and validation using weather radar observations. *Journal of Geophysical Research*, 114, 2009.

J. Schmetz, Y. Govaerts, M. König, H.J. Lutz, A. Ratier, and S. Tjemkes. A short introduction to meteosat second generation (msg). Technical report, EUMETSAT, 2002.

URL <http://www.eumetsat.int>.

E.L.A. Wolters, H.M. Deneke, R.A. Roebeling, and A.J. Feijt. Comparison of sevir and modis clouds phase determination over mid-latitude regions.

*Algorithm Theoretical Basis Document for SAFNWC/MSG Precipitating Cloud (PC-PGE04 v1.5)*, 2012.

*Product User Manual for SAFNWC/MSG Precipitating Cloud (PC-PGE04 v1.5)*.

*Algorithm Theoretical Basis Document for Convective Rainfall Rate (CRR-PGE05 v3.1.1)*.

R.A. Roebeling, E.L.A. Wolters, J.F. Meirink, and H. Leijnse. Triple collocation of summer precipitation retrievals from sevir over europe with gridded rain gauge and weather radar data. *Journal of Hydrometeorology*, 13, 2012.

R.A. Roebeling, A.J. Feijt, and P. Stammes. Cloud property retrievals for climate monitoring: Implications of differences between spinning enhanced visible and infrared imager (sevir) on meteosat-8 and advanced very high resolution radiometer (avhrr) on noaa-17. *Journal of Geophysical Research*, 111, 2006.

URL [http://msgcpp.knmi.nl/mediawiki/index.php/MSGCPP\\_product\\_description](http://msgcpp.knmi.nl/mediawiki/index.php/MSGCPP_product_description).

I. Holleman. Bias adjustment and long-term verification of radar-based precipitation estimates. *Meteorological Applications*, 14:195–203, 2007.

A. Overeem. *Climatology of extreme rainfall from rain gauges and weather radar*. PhD thesis, Wageningen University, 2009.

A. Overeem, I. Holleman, and A. Buishand. Derivation of a 10-year radar-based climatology of rainfall. *Journal of Applied Meteorology and Climatology*, 48:1448–1463, 2009.

P. Hazenberg, H. Leijnse, and R. Uijlenhoet. Radar rainfall estimation of stratiform winter precipitation in the belgian ardennes. *Water Resources Research*, 47, 2011.

I. Holleman. Bias adjustment of radar-based 3-hour precipitation accumulations. Technical report, KNMI, 2006.

URL [http://www.knmi.nl/~beekhuis/index.php?show=rad\\_intro.html](http://www.knmi.nl/~beekhuis/index.php?show=rad_intro.html).



R. Roebeling. *Cloud Physical Properties Retrieval for Climate Studies*. PhD thesis, Buys Ballot Onderzoekschool (BBOS), 2008.

R. Amorati, P.P. Alberoni, V. Levizzani, and S. Nanni. Ir-based satellite and radar rainfall estimated of convective storms over northern italy. *Meteorological Applications*, 7, 2000.

J. Vivekanandan, B.E. Martner, M.K. Politovich, and G. Zhang. Retrieval of atmospheric liquid and ice characteristics using dual-wavelength radar observations. *IEEE Transactions on Geoscience and Remote Sensing*, 37(5), 1999.

URL <http://trmm.gsfc.nasa.gov/>.